Supplementary Information (SI) for Chemical Communications.

Supporting information

The decarboxylative and dehydrogenative coupling of formate: from anisyl formate to a high value-added diamine

Yichao Wang[ab], Hongchen Cao[ab], Shiwen Yang[a], Leilei Zhang*[a], Rui Wang[a], Aiqin Wang*[a] and Tao Zhang*[a]

[a.] CAS Key Laboratory of Science and Technology on Applied Catalysis, Dalian Institute of Chemical Physics, Chinese Academy of Sciences, Dalian 116023, Liaoning, China.

[b.] University of Chinese Academy of Sciences, Beijing 100049, China.

Email: zhangleilei@dicp.ac.cn; aqwang@dicp.ac.cn; taozhang@dicp.ac.cn

Table of Contents

1. Materials and Characterizations

1.1 Materials

Anisyl formate, hexafluoroisopropanol (HFIP), benzyl alcohols, hydroxylapatite (HAP, 100 nm), γ-Al_2O_3 (10 nm), 5 wt% Pd/C, 5 wt% Ru/C, and 5 wt% Pt/C were purchased from Aladdin. Al_2O_3 (3 mm pellet) was obtained from Alfa Aesar. SiO_2 (AEROSIL OX 50) was produced by EVONIK. Ruthenium nitrosyl nitrate (1.5w/v, in H_2O) was come from Macklin. HNO_3 (68 wt%) and other chemicals were bought from Damao Chemical Reagent Factory in analytically pure grade.

Procedures for synthesis of benzyl formate[1]: 40.0 mmol acetic anhydride and 50.0 mmol formic acid were sequentially added into a flask and stirred at 60 °C for 1 h. The resulting mixed anhydride was cooled to room temperature. Afterward, 5.0 mmol benzyl alcohol and 10.0 mmol $NaHCO_3$ were added. When the substrate was consumed, the reaction was quenched by water/ethyl acetate and extracted by ethyl acetate for 2 times. The combined organic phase was washed with water and brine, dried over anhydrous Na_2SO_4, and concentrated under vacuum. The crude product was purified through silica gel column and the pure benzyl formate was dissolved in THF for further reaction. The substrate structure was confirmed through mass spectrometry (m/z + 28 compared with the benzyl alcohol).

1.2 Characterizations

Powder X-ray diffraction patterns: XRD experiments of different catalysts were performed on a X'pert Pro-1 diffractometer (PANAlytical). Operation conditions: Cu Kα radiation source ($\lambda = 0.15432$ nm) working at 40 kV and 40 mA, 2θ ranges from 5 to 80°.

Inductively coupled plasma optical emission spectroscopy: ICP-OES analyses of ruthenium loadings of different catalysts were accomplished on an Avio 550 Max spectrometer.

High resolution transmission electron microscopy: HRTEM images were picked on a JEM-2100F transmission electron microscope (operating voltage: 200 kV) equipped with an EDS microanalysis system. Catalysts were pre-ultrasonicated for 15 min in ethanol and dropped onto Cu grids before drying by a heating stage.

Aberration-corrected high-angle annual dark-filed scanning transmission electron microscopy: AC-HAADF-STEM pictures were obtained on a JEOL JEM-ARM200F electron microscope with a CEOS probe corrector and a guaranteed resolution of 0.08 nm. Catalysts were pre-ultrasonicated for 20 min in ethanol and dropped onto Cu grids before drying by a heating stage.

X-ray photoelectron spectroscopy: XPS experiments were performed on a Thermo ESCALAB 250Xi instrument. Operation conditions: Al Kα X-ray radiation source (hν = 1486.6 eV) working at 15 kV and 10.8 mA. The binding energy calibration was based on polluted C 1s signal (284.6 eV). All samples were tableted as small flakes with thickness less than 2 mm and diameters larger than 5 mm. For the in situ experiment, the passivated catalyst was reactivated in the cavity under H_2 flow at 190 °C for 2 h before measurement.

In situ Raman spectroscopy: In situ Raman experiments were accomplished on a NanoWizard Raman spectrometer equipped with a 532 nm laser. The catalyst was in situ reduced at 400 °C for 1 h under 30 mL/min H_2. The spectra were collected at 25 °C.

In situ electron paramagnetic resonance (EPR) spectroscopic measurements were carried out on a Bruker A200 EPR spectrometer. The catalyst was pre-reduced in an in-situ reaction tube at 400 °C for 1 h under 30 mL/min H_2 and tested under room temperature.

Nitrogen sorption isotherms: The surface area was measured on an ASAP 2460 physisorption analyzer based on Brunauer–Emmett–Tertiott (BET) method. The samples were pre-degassed for 12 h under vacuum at 200 °C.

CO_2 and NH_3-temperature-programmed desorption: CO_2-TPD and NH_3-TPD experiments were conducted on the AutoChem II 2920 (Micromeritics Instruments Co., Ltd) equipped with an on-line mass spectrometer. 100 mg catalyst was used for every experiment and the catalyst was pre-reduced at 400 °C for 1 h under 30 mL/min H_2. 5% CO_2/He and pure NH_3 were used as analysis gases. Heating program: 10 °C /min from 100 to 800 °C.

H_2-temperature-programmed desorption: The freshly prepared catalyst was reduced in situ under 30 mL/min H_2. Heating program: 10 °C/min, 400 °C, 1 h. At the same time, this process was monitored by an on-line mass spectrometer. After the reduction, the catalyst was cooled down to 50 °C and purged by He for 30 min. H_2-TPD spectra were then collected under a 10 °C /min heating rate from 50 to 800 °C.

In situ diffuse reflection infrared Fourier transform spectroscopy: DRIFT experiments including Ester-DRIFTS and O_2-DRIFTS were collected on an INVENIO spectrometer (Bruker Optics GmbH &Co. KG) equipped with a mercury-cadmium-telluride (MCT) detector. The spectra were acquired under conditions of 4 cm^{-1} resolution from 4000 to 600 cm^{-1}, 32 scans, and 10 min interval for each two spectra. Before measurement, catalysts were pre-reduced at 400 °C for 1 h under 30 mL/min H_2.

For Ester-DRIFTS, about 3 μL anisyl formate was introduced onto the catalyst surface through a syringe at 25 °C under the protection of He after the background signal was collected. Physically adsorbed ester was purged by continuous He flow (50 mL/min). For blank sample, KBr was loaded instead.

For O_2-DRIFTS, the spectra were recorded under 30 mL/min 1% O_2/N_2.

Differential scanning calorimetry: DSC analysis of the polymer was performed on a TGA 55 differential scanning calorimeter (TA Instruments).

Thermal gravimetric analysis: TGA analysis of the polymer was performed on a DSC25 thermal gravimetric analyzer (TA Instruments).

Gel permeation chromatography: GPC analysis of the polymer was performed on a Waters 1515GPC gel permeation chromatographer (Waters Corporation).

Nuclear Magnetic Resonance spectroscopy: NMR spectra were collected on a JNM-ECZL400S nuclear magnetic resonance spectrometer. About 20-30 mg samples were dissolved in 0.5 mL deuterium reagent.

Extended X-ray adsorption fine structure (EXAFS) and X-ray absorption near edge structure (XANES) were collected at the Shanghai Synchrotron Radiation Facility (SSRF, BL14W1 beamline). About 200 mg $Ru_{5wt\%}/MoS_2$ catalyst was pre-reduced under hydrogen atmosphere at 400 °C for 1 h, loaded into a polytetrafluoroethylene mold with a thickness of 2 mm, and sealed into a thermoplastic bag under argon atmosphere. The experiment was conducted at room temperature under transmission mode and the raw data was processed with the Athena software.

2. Catalyst Preparations

Ru/SiO_2: 0.5 g SiO_2 was first dispersed into 20 mL methanol under sonication for 30 min. Then the pre-determined amount of ruthenium nitrosyl nitrate in 5 mL water was added under stirring during 15 min in dropwise. The mixture was stirred for another 12 h at room temperature and excess solvent was evaporated in an 80 °C water bath. The resulting precursor was grinded into fine powder, dried at 120 °C for 12 h, and calcinated in the muffle oven in static air under 400 °C for 2 h at a ramping rate of 5 °C/min. For $Ru_1Mo_{0.5}/SiO_2$ catalyst, a mixed solution of Ru and Mo (ammonium molybdate hydrate) was used.

Hydroxylapatite and γ-Al_2O_3 supports were used for preparing the corresponding Ru/HAP and Ru/γ-Al_2O_3 catalysts following the same procedures as in Ru/SiO_2. All commercial supports were calcinated in muffle oven at 500 °C for 2 h before use.

In_2O_3[2]: 24.4 g $In(NO)_3 \cdot 4.5H_2O$ was first dissolved into 100 mL water and 280 mL ethanol under stirring. A mixture of 70 mL NH_3 solution (25 wt% in water) and 220 mL ethanol was used as precipitator and added into the above In solution using a constant flow pump during 1 h. After aging at 80 °C for 3 h, the precipitation was purified by water and ethanol, dried at 80 °C overnight, and calcinated at 500 °C for 3 h in static air.

Ru/In_2O_3[3]: 0.495 g In_2O_3 was added into 50 mL aqueous solution of ruthenium nitrosyl nitrate at room temperature. The mixture was sonicated for 30 min and stirred for another 30 min. Next, 0.36 g urea was added into the mixture and the liquid temperature was raised to 80 °C. After aging at the same temperature for 3 h, the precipitation was flittered and washed with deionized water. The catalyst was obtained after drying in a vacuum oven for 12 h at 60 °C.

MoS_2: 2.47 g $(NH_4)_6Mo_7O_{24}\cdot 4H_2O$ and 2.13 g thiourea were dissolved in 80 mL ultra-pure water under stirring in a 110 mL Teflon lining. 30 mg L-ascorbic acid was then added into the solution. The system was transferred into a hydrothermal reactor and sealed tightly. The reactor was heated to 200 °C in 30 min and kept for 18 h in a muffle oven. After cooling down to the room temperature naturally, the black precipitate was flittered, washed with water and ethanol, and dried in a 60 °C oven for 12 h.

Ru/MoS_2: First, 1 g MoS_2 support and 5 g H_2O were weighted into a mortar and grinded moistly for 10 min. Thereafter, 10 mL H_2O was added and the supernatant homogenous dispersion liquid of MoS_2 was transferred into a 250 mL baker using a dropper. Repeating the grinding—water leaching—suction process until all MoS_2 was transferred into the baker in the form of uniform dispersion liquid. The precise amount of ruthenium nitrosyl nitrate based on loadings (0.5 wt%, 1 wt%, 2 wt%, and 5 wt%) was dissolved into 10 mL water and added into the above MoS_2 dispersion liquid. The mixture was stirred at 80 °C overnight until the evaporation of H_2O. The black powder was treated at 200 °C for 2 h in a muffle oven. Before the reaction, the catalyst was reduced at 400 °C for 1 h (pure H_2) and passivated at room temperature for another 1 h (1% O_2/N_2).

Ru/MoS_2-Nano particle: Preparation of ruthenium nanoparticles: 0.104 g $RuCl_3\cdot xH_2O$ was dissolved into 25 mL ethylene glycol in a 100 mL three-neck round-bottom flask under stirring (500 rpm) at room temperature. Then 25 mL 0.5 $mol\cdot L^{-1}$ ethylene glycol solution of sodium hydroxide was added and the resulting mixture was stirred at room temperature (500 rpm) for 15 min. The flask was transferred into a 160 °C oil bath and maintained for 1.5 h at 500 rpm. The solution was bubbled by 15 mL/min Ar during the heating process for timely removal of low-boiling point byproducts. Preparation of the supported nanoparticle catalyst: 0.5 g hydrothermally synthesized MoS_2 was dispersed in 10 mL acetone under sonification for 30 min, during which the predetermined amount of ruthenium nanoparticle solution was weighted, diluted by ×20 volume 1M HCl aqueous solution, and extracted by 5 mL ethyl acetate. The ethyl acetate phase was then added into the MoS_2 dispersion liquid under stirring and the mixture was dried in a 50 °C water bath. Finally, the catalyst was collected and reduced at 400 °C for 1 h under hydrogen atmosphere.

3. Reaction procedures

The decarboxylative and dehydrogenative coupling of anisyl formate was performed in a 50 mL reactor made of steel 316. In a typical reaction, 50 mg catalyst, 8 mmol anisyl formate, 8 mL THF, 1 mL CH_3CN, and n-dodecane internal standard were first loaded into the reactor under the protection of Ar. After sealing, the atmosphere in the reactor was replaced by N_2 for three times. The heating program was set as below: 6 °C/min from room temperature (r.t.) to 190 °C, holding for 8 h, and cooling down to r.t. naturally. The stirring rate was set as 500 rpm. After the reaction, the liquid and gas products were collected through a filter (nylon 66) and a gas bag, respectively.

The nitration of 1,2-bis(4-methoxyphenyl) ethane: 5 mmol 1,2-bis(4-methoxyphenyl) ethane was dissolved into 50 mL hexafluoroisopropanol (HFIP) under ultrasonication in a 250 mL baker. The solution was cooled in an ice bath and 10 mmol HNO_3 (68 wt% in water) in another 50 mL HFIP was added in dropwise during 30 min. After the addition, the reaction system was immediately evaporated under reduced pressure in a 25 °C water bath. The resulting yellow solid was washed in turn by water and ethanol for three times. The final product, 1,2-bis(4-methoxy-3-nitrophenyl) ethane, was received after drying in Ar flow at 50 °C for 6 h.

The reduction of 1,2-bis(4-methoxy-3-nitrophenyl) ethane: 80 mg 5 wt% Pt/C (containing 40-60 wt% water), 500 mg 1,2-bis(4-methoxy-3-nitrophenyl) ethane, and 20 mL ethanol were loaded into a 50 mL reactor. The system was purged by Ar for three times and charged with 3.5 MPa H_2. The reaction was performed at 30 °C for 8 h. After the reaction, $MgSO_4$ was added into the reactor to remove the produced water. The ethanol phase was collected into a 50 mL round bottom flask by filtration and dried under the flow of Ar at 50 °C. The pure product, 5,5'-(ethane-1,2-diyl) bis(2-methoxyaniline), was collected and stored under Ar.

The preparation of semiaromatic polyamide: 1 mmol 5,5'-(ethane-1,2-diyl) bis(2-methoxyaniline), 1 mmol adipic acid, 0.5 mL pyridine, 1 mL triphenyl phosphite, and 0.15 g $CaCl_2$ were added into a 10 mL three-neck round-bottom flask. Afterwards, 10 mL N-Methyl-2-pyrrolidone was added and the reaction system was heated to 120 °C and maintained for 3 h. The yellow color lightened as the reaction progressed. After the reaction, the solution was dropped into ethanol (× 20 volume) for precipitation. The milk white product was flittered, washed, dried, and grinded.

Kinetic isotope effect (KIE) was measured in the same reactor as in the reaction test. 10 mg $Ru_{5wt\%}/MoS_2$ catalyst, 4 mmol anisyl formate, 16 mL THF, 2 mL CH_3CN, and n-dodecane were loaded into the reactor under the protection of Ar. Then 1 MPa Ar was charged and the reactor was heated to 190 °C at a ramping rate of 6 °C/min (500 rpm). Timing began once the reactor reached the targeted temperature. About 0.5 mL liquid was picked every 10 min and analyzed by GC. For accuracy, the conversion rate was kept below 5 %.

4-methoxybenzyl 2-oxoacetate was synthesized following the reported procedures without any modifications[4].

The conversion of substrates and the yield of products were calculated by using the following equations:

$$\text{Conversion} = \frac{consumed\ \text{moles of substrate}}{\text{moles of substrate}} \times 100\ (\%) \text{...........Equation 1}$$

$$\text{Yield} = \frac{\text{moles of product}\ (\times 2\ in\ case\ of\ dimer\ product)}{\text{moles of substrate}} \times 100\ (\%) \text{...........Equation 2}$$

4. Supplementary Tables and Figures

Table S1 The catalytic performances of different homogeneous Ru catalysts.

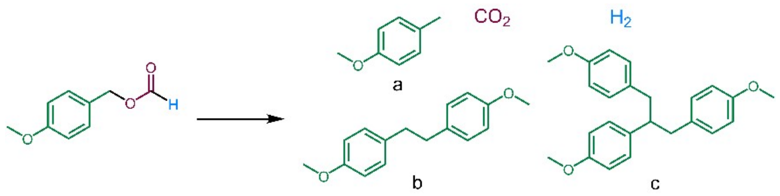

Entry	Cat.	Conv./ %	Yield/ %		
			a	b	c
1	$Ru_3(CO)_{12}$	18.8	4.4	0	0
2	$RuCl_3$	83.9	14.1	7.9	0
3	$Ru(PPh_3)_3Cl_2$	51.4	29.0	5.7	0
4	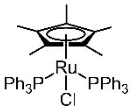	37.0	5.7	2.1	0
5	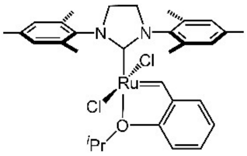	82.4	38.3	12.1	0

Reaction conditions: 5 mol% catalyst, 3 mmol anisyl formate, 8 mL THF, 1 mL CH_3CN, 190 °C, 2 h, N_2, 500 rpm.

Table S2 The substrate scope of the $Ru_{5wt\%}/MoS_2$ catalyst.

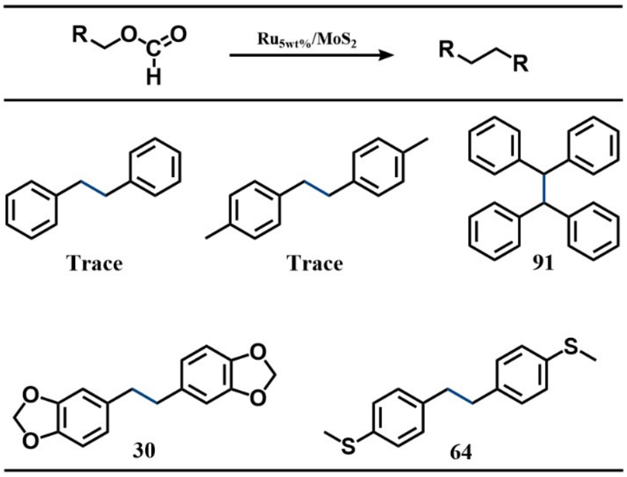

Reaction conditions: 50 mg $Ru_{5wt\%}/MoS_2$, 3 mmol formate, 8 mL THF, 1 mL CH_3CN, 190 °C, 8 h, 500 rpm, N_2. Isolated yields were given.

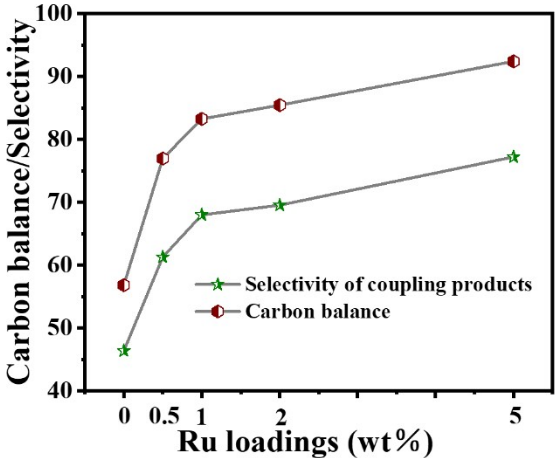

Fig. S1 The change of product selectivity and carbon balance as a function of Ru loadings. Reaction conditions: 50 mg catalyst, 8 mmol anisyl formate, 8 mL THF, 1 mL CH_3CN, 190 °C, 8 h, N_2, 500 rpm.

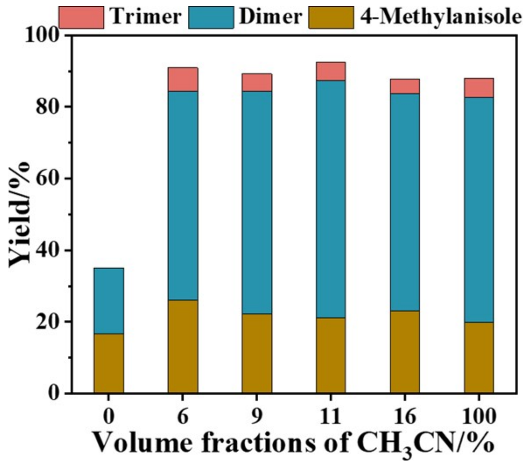

Fig. S2 The optimization of acetonitrile ratio in the mixed solvent. The volume fraction of CH_3CN = $V_{Acetonitrile}/(V_{Acetonitrile} + V_{THF})$. Reaction conditions: 50 mg $Ru_{5wt\%}/MoS_2$, 8 mmol anisyl formate, 9 mL solvent (THF + CH_3CN), 190 °C, 8 h, N_2, 500 rpm.

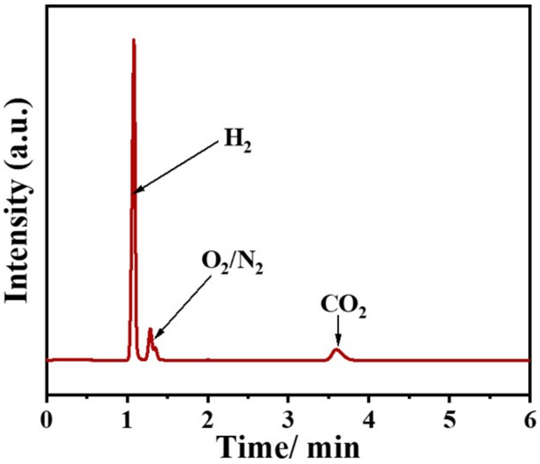

Fig. S3 The GC spectrum of collected gas products after the reaction (corresponding to **Table 1**, entry 10, detector: TCD, carrier gas: Ar). The molar ratio between H_2 and CO_2 was about 7: 10 (H_2: CO_2).

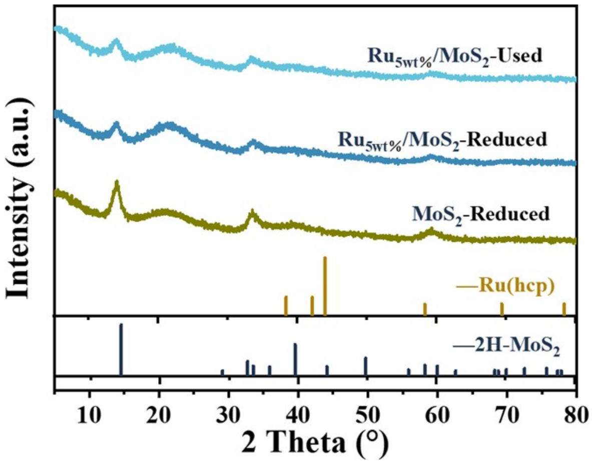

Fig. S4 X-ray diffraction patterns of different catalysts.

Table S3 ICP-OES tests of $Ru_{5wt\%}/MoS_2$ catalysts in different stages.

Contents of Ru (wt%)	**As-synthesized**	**After reduction**	**After reaction**
	4.4	**4.7**[a]	**4.7**

[a] Ascribed to the decomposition of Ru precursor and loss of water.

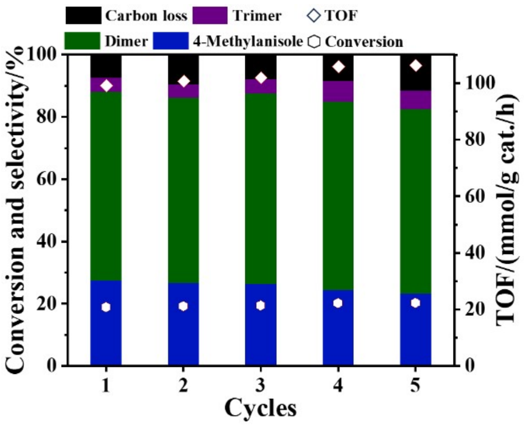

Fig. S5 The recycling experiment of the $Ru_{5wt\%}/MoS_2$ catalyst. Reaction conditions: 50 mg $Ru_{5wt\%}/MoS_2$, 8 mmol anisyl formate, 8 mL THF, 1 mL CH_3CN, 190 °C, 20 min, N_2, 500 rpm. After each cycle, the catalyst was washed by CH_2Cl_2, dried at room temperature, and used for the next reaction.

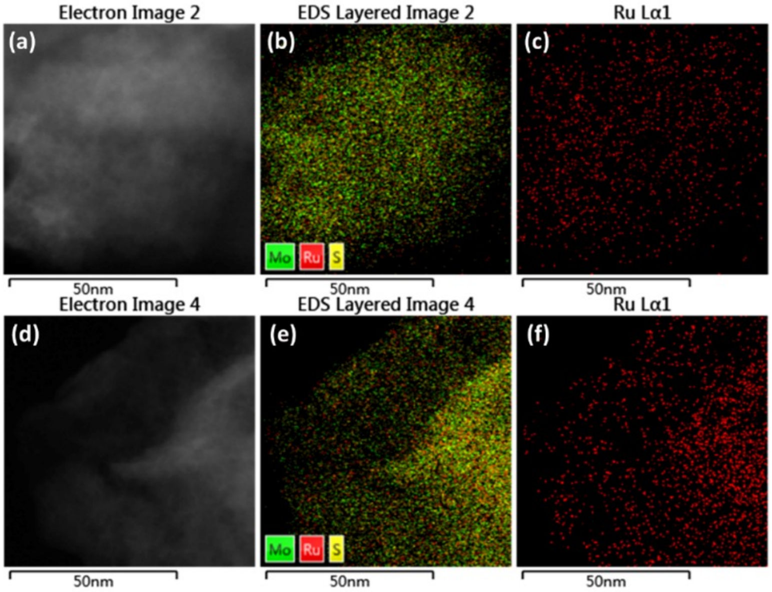

Fig. S6 STEM images and the corresponding EDX mapping results of the fresh (a-c) and used (d-f) $Ru_{5wt\%}/MoS_2$ catalysts.

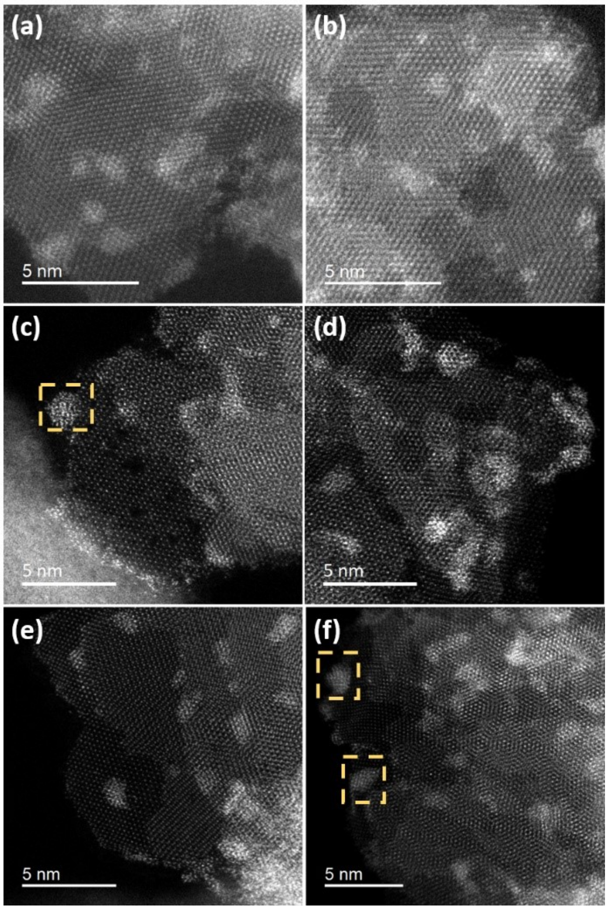

Fig. S7 AC-HAADF-STEM images of $Ru_{5wt\%}/MoS_2$ catalysts: (a, c-f) The fresh catalyst, (b) The used catalyst. Box: Ru nanoclusters.

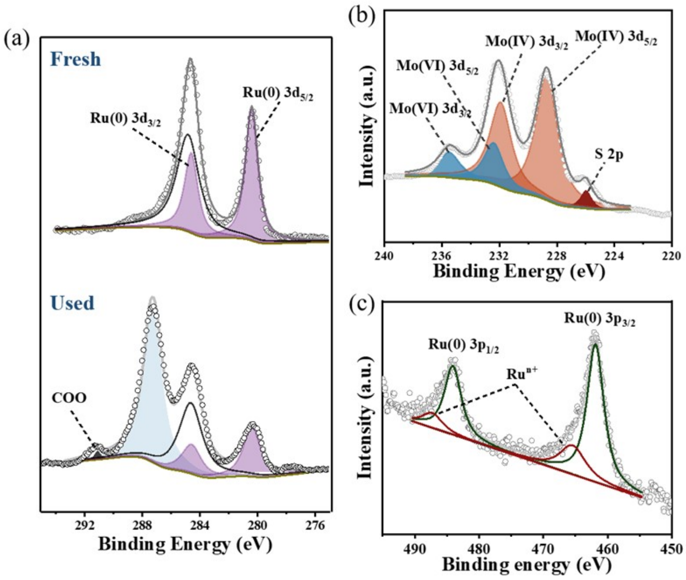

Fig. S8 (a) C1s and Ru 3d XP spectra of the fresh and used $Ru_{5wt\%}/MoS_2$ catalysts. (b) The Mo 3d and (c) Ru 3p XP spectra of the used $Ru_{5wt\%}/MoS_2$ catalyst. The C1s peak emerged at 291.2 eV after the reaction could be identified as the COO species[5].

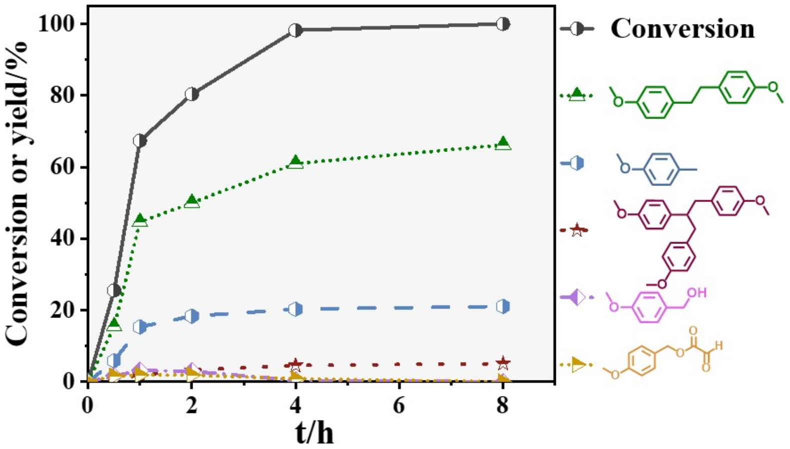

Fig. S9 The reaction time profile of the decarboxylative and dehydrogenative coupling of anisyl formate catalyzed by the $Ru_{5wt\%}/MoS_2$ catalyst. Reaction conditions were as same as in **Table 1**, entry 10.

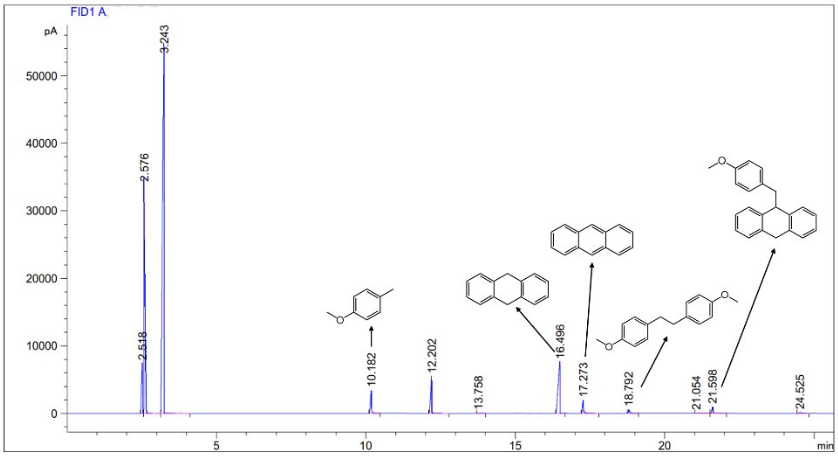

Fig. S10 The GC spectrum of the radical trapping experiment. Reaction conditions: 3 mmol anisyl formate, 4.5 mmol 9,10-dihydroanthracene, 8 mL THF, 1 mL CH_3CN, 190 °C, 500 rpm, N_2.

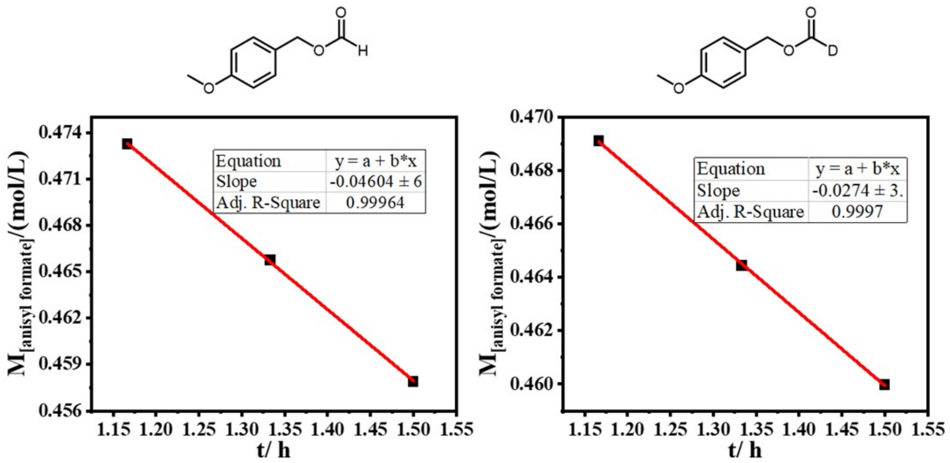

Fig. S11 KIE measurements.

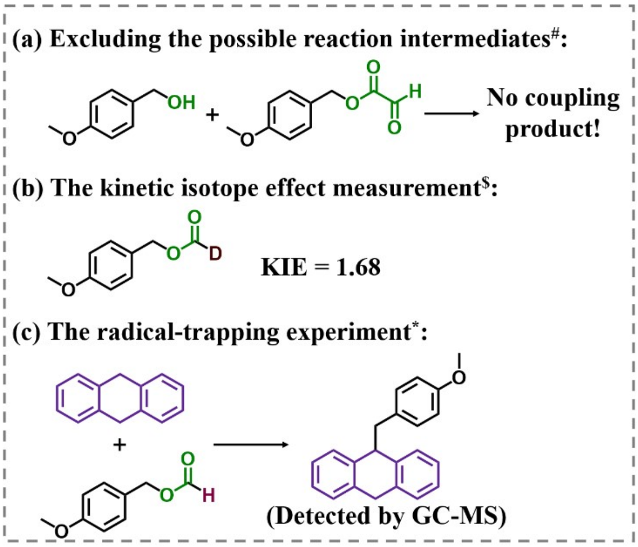

Scheme S1 Complementary experiments for illustrating the reaction mechanism. #Reaction conditions: 50 mg $Ru_{5wt\%}/MoS_2$, 4 mmol anisyl alcohol, 4 mmol 4-methoxybenzyl 2-oxoacetate, 8 mL THF, 1 mL CH_3CN, 190 °C, 8 h, N_2, 500 rpm; $The conversion rate was controlled below 5%, as seen in **Fig. S11**; *As seen in **Fig. S10**.

(a) Secondary reactions between products$^{\#}$:

Substrate \ Product	Monomer/%	Dimer/%	Trimer/%
Monomer	Recovered	——	——
Dimer	——	Recovered	——
Monomer and dimer	Recovered	Recovered	——

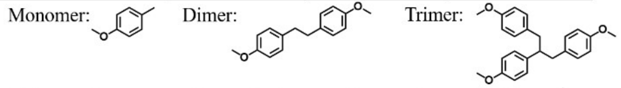

(b) Secondary reactions between formate and dimer$^{\$}$:

Substrate \ Product	Conv./%	Monomer/%	Dimer/%	Trimer/%
Anisyl formate	100	18.8	63.9	3.6
Anisyl formate and Dimer	51.6	11.8	——	4.7

(c) The crossover experiment*:

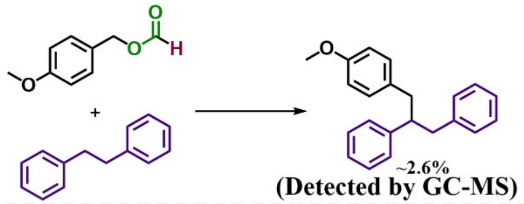

Scheme S2 Validation experiments for revealing the mechanism of trimer formation. Reaction conditions: 50 mg $Ru_{5wt\%}/MoS_2$ catalyst, 8 mL THF, 1 mL CH_3CN, 190 °C, 500 rpm, N_2. Substrates and reaction time: $^{\#}$3 mmol substrate (monomer, dimer, or mixture), 12 h; $^{\$}$3 mmol anisyl formate or 3 mmol anisyl formate and 1.5 mmol dimer, 2 h; *3 mmol anisyl formate and 1.5 mmol bibenzyl, 12 h.

Further reactions of monomer, dimer, and their mixture were ruled out (**Scheme S2(a)**). Furthermore, we added 0.5 equiv. dimer into the reaction system accompanied with anisyl formate to distinguish the possible reaction between the formate and dimer. Notably, a suppressed conversion of anisyl formate was captured (51.6% vs 100% in **Scheme S2(b)**), which may come from the competitive adsorption between dimer and formate on the catalytic surface. However, a slight pronounced trimer production was given even under lower conversion, implying the possible secondary reaction between dimer and formate. A crossover experiment was then designed by introducing bibenzyl into the reaction system and a critical coupling product containing both parts of anisyl formate and bibenzyl was captured (**Scheme S2(c)**). Based on these control experiments, we speculate that the trimer product may derive from the secondary reaction between anisyl radical and dimer, which is in agreement with the reactivity of benzyl radical described in the literature[6].

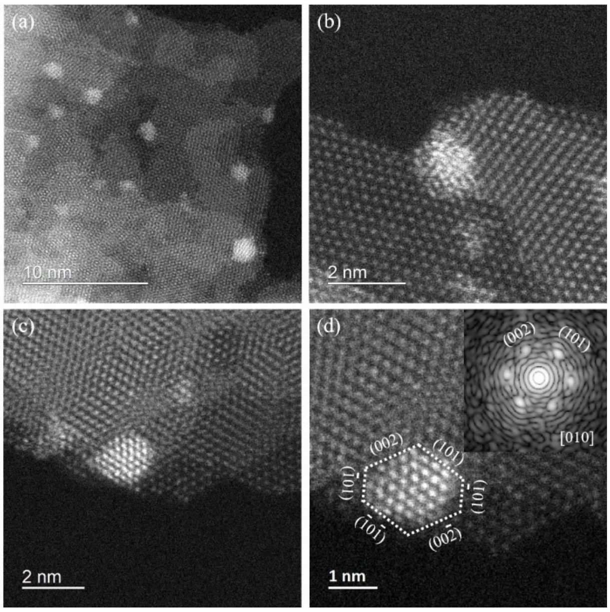

Fig. S12 Representative AC-HAADF-STEM images of the freshly prepared $Ru_{0.5wt\%}/MoS_2$-Nano particle catalyst.

Table S4 The reaction rates of contrast single atom and nano particle catalysts.

Cat.	**Initial reaction rate (mmol/g cat./ h)**	**4-Methylanisole (mmol/g cat./ h)**	**1,2-Bis(4-methoxyphenyl) ethane (mmol/g cat./ h)**	**1,2-bis(4-methoxyphenyl) ethane/ 4-Methylanisole**
$Ru_{0.5wt\%}/MoS_2$-Single atom	6.6	1.8	0.8	0.44
$Ru_{0.5wt\%}/MoS_2$-Nano particle	5.3	1.6	0.6	0.38

Reaction conditions: 50 mg catalysts, 8 mL THF, 1 mL CH_3CN, 190 °C, 30 min, N2, 500 rpm.

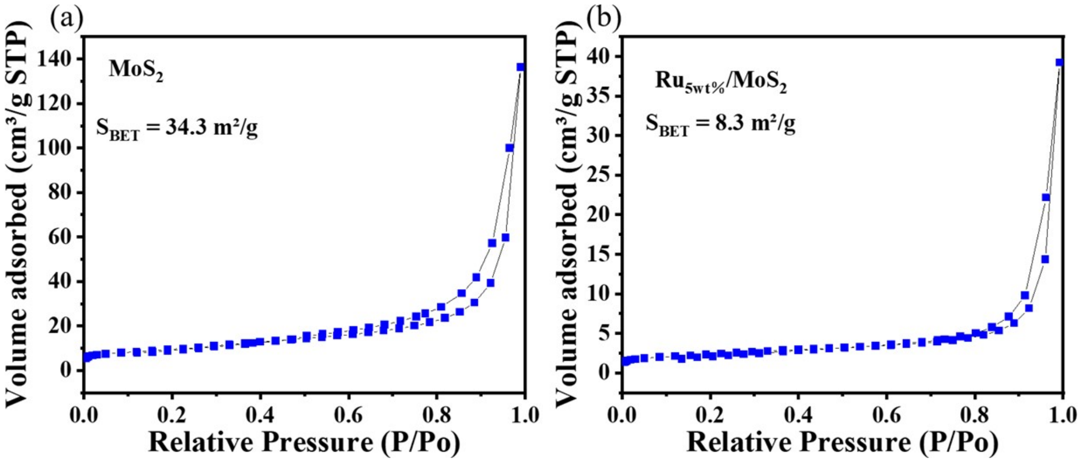

Fig. S13 N_2 adsorption-desorption isotherms of (a) MoS_2 and (b) $Ru_{5wt\%}/MoS_2$ catalysts.

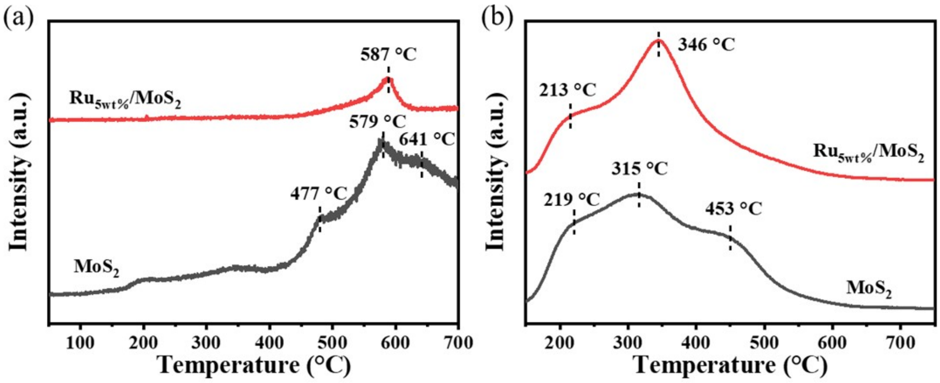

Fig. S14 (a) The CO_2-TPD and (b) NH_3-TPD results of MoS_2 and $Ru_{5wt\%}/MoS_2$ catalysts.

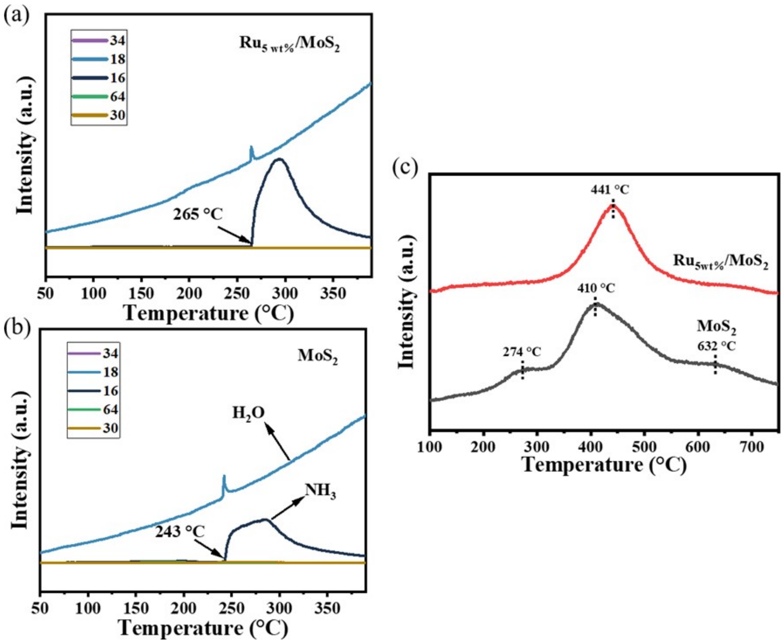

Fig. S15 (a-b) The tracking of the reduction process of MoS_2 and $Ru_{5wt\%}/MoS_2$ catalysts using mass spectroscopy. (c) H_2-TPD results. Mass signals: H_2S, 34; H_2O, 18; NH_3, 16; SO_2, 64; NO, 30.

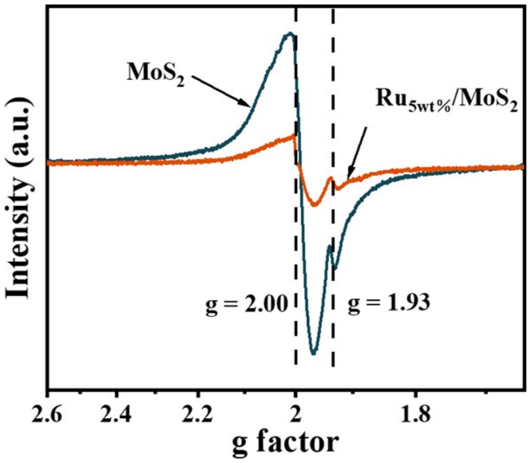

Fig. S16 In situ EPR experiments of MoS_2 and $Ru_{5wt\%}/MoS_2$ catalysts. The signal at g = 2.00 can be ascribed to Mo-S dangling bonds, g = 1.93 may originate from Mo species in lower oxidation or undercoordinated states[7,8].

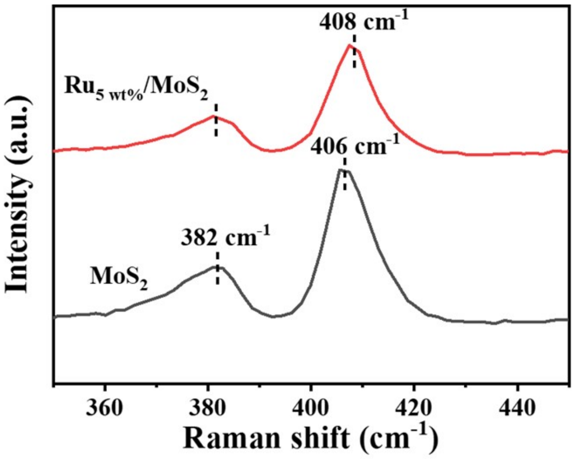

Fig. S17 In situ Raman experiments of MoS_2 and $Ru_{5wt\%}/MoS_2$ catalysts. Peaks at approximately 382 and 405 cm^{-1} for MoS_2 sample come from the vibration modes of in-plane E^1_{2g} and out-of-plane A_{1g}, respectively[9]. The red-shift of these two bands was used as a criterion in the literature for more vacancy generation[10], but no obvious shifts were captured in these two samples.

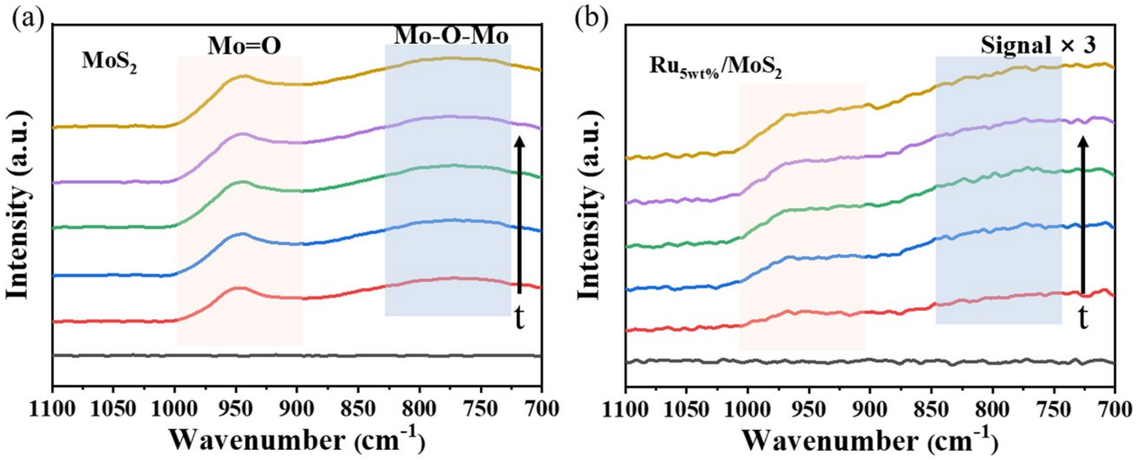

Fig. S18 In situ O_2-DRIFTS spectra of MoS_2 and $Ru_{5wt\%}/MoS_2$ catalysts. The sulfur vacancy types: Mo=O represents edge sulfur vacancy and Mo-O-Mo represents in-plane sulfur vacancy[11].

Table S5 The activity of $Ru_1Mo_{0.5}/SiO_2$ catalyst.

Cat.	**Conv. (%)**	**4-Methylanisole (%)**	**1,2-bis(4-methoxyphenyl) ethane (%)**	**Trimer (%)**
$Ru_1Mo_{0.5}/SiO_2$	76.0	17.4	37.9	3.1

Reaction conditions: 50 mg catalyst, 3 mmol anisyl formate, 8 mL THF, 1 mL CH_3CN, 190 °C, 2 h, N_2, 500 rpm.

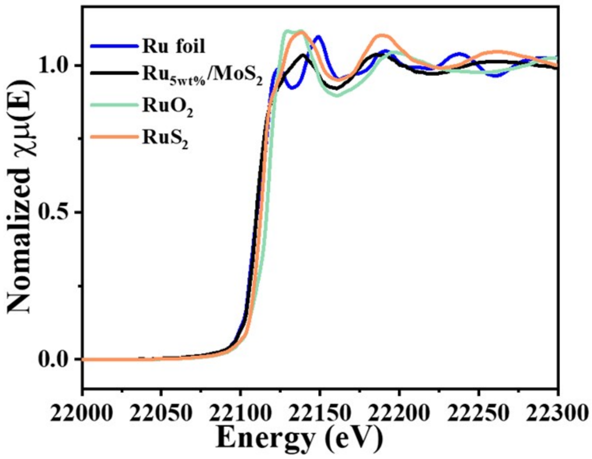

Fig. S19 Normalized NEXAS spectra of the Ru K-edge for the Ru$_{5wt\%}$/MoS$_2$ catalyst and standard samples.

Table S6 E$_0$ value of the Ru$_{5wt\%}$/MoS$_2$ catalyst and standard samples

Entry	Cat.	E$_0$
1	Ru foil	22117.0
2	RuS$_2$	22117.9
3	RuO$_2$	22118.0
4	Ru$_{5wt\%}$/MoS$_2$	22117.2

The E$_0$ was derived from the peak value of the first derivative of XANES.

Table S7 Curvefit Parametes^a for Ru K-edge EXAFS for samples.

Sample	Path	R(Å)	N	ΔE$_0$ (eV)	□^{2}(Å^2)	R factor (%)
Ru foil	Ru - Ru	2.67+/-0.00	12^b	2.4+/-0.9	0.003+/-0.001	1.1
Ru$_{5wt\%}$/MoS$_2$	Ru - S	2.34+/-0.01	5.1+/-0.5	0.9+/-1.0	0.004+/-0.001	1.1
	Ru – Ru (Mo)	2.68+/-0.01	2.2+/-0.6		0.004+/-0.001	

$^a S_0^2$ was fixed as 0.72. Data ranges: $3.0 \le k \le 10.7$ Å^{-1}, $1.0 \le R \le 3.0$Å. The variable parameters number is 6, out of a total of 9.6 independent data points for these samples. ^{b}The coordination number for Ru-Ru was fixed as 12 based on Ru foil crystal structure (Ru mp-8639). The variable parameters number is 4, out of a total of 9.6 independent data points for Ru foil sample.

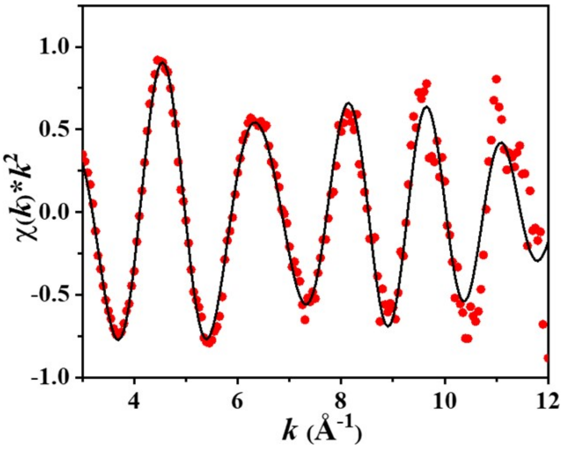

Fig. S20 Ru K-edge EXAFS (points) and the curvefit (line) for the $Ru_{5wt\%}/MoS_2$, shown in k^2 weighted *k*-space.

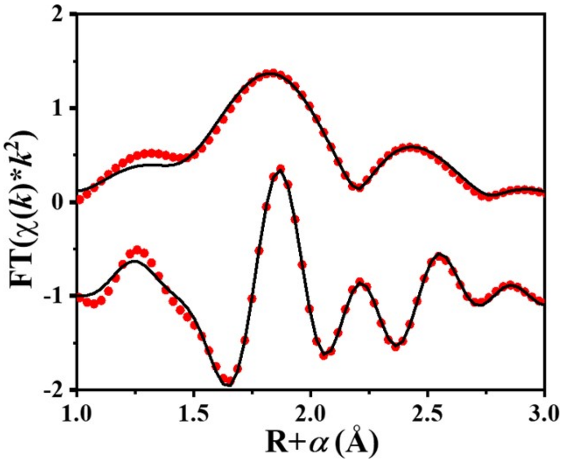

Fig. S21 Ru K-edge EXAFS (points) and curvefit (line) for the $Ru_{5wt\%}/MoS_2$, shown in *R*-space (FT magnitude and imaginary component). The data is k^2 weighted and not phase-corrected.

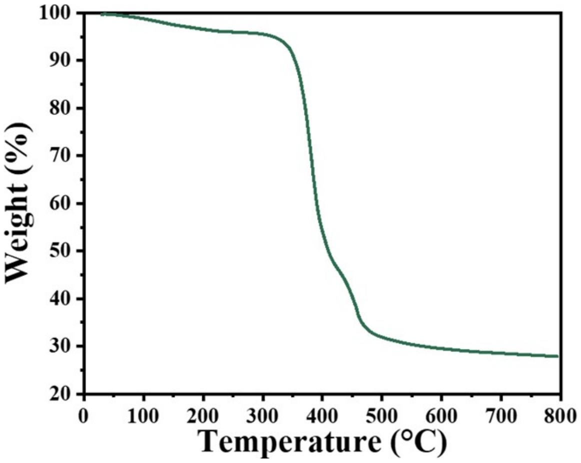

Fig. S22 TGA analysis of the synthesized semiaromatic polyamide (sample in **Fig. S24(a)**).

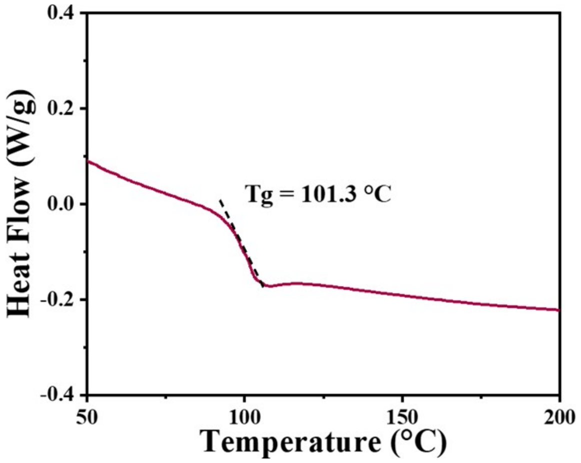

Fig. S23 DSC analysis of the synthesized semiaromatic polyamide (sample in **Fig. S24(a)**).

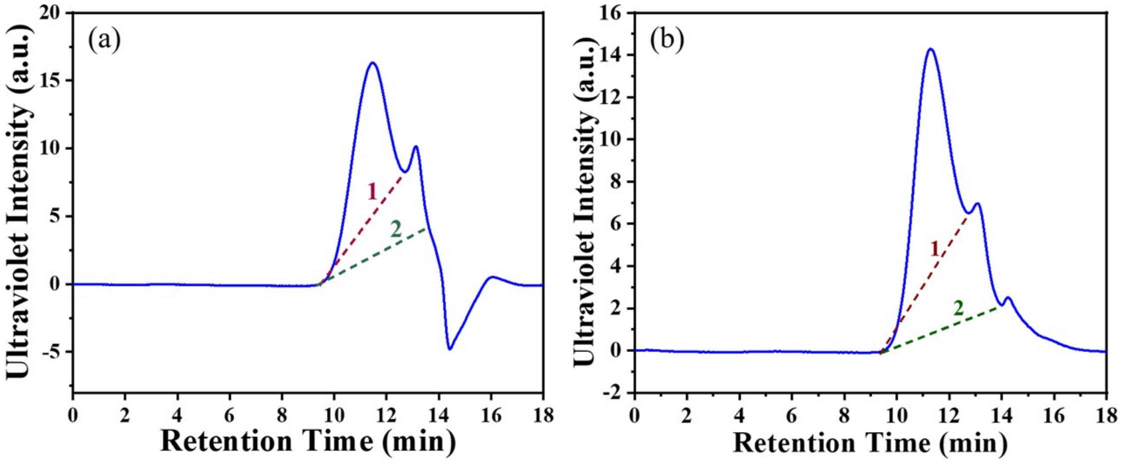

Fig. S24 GPC analyses of the synthesized semiaromatic polyamides. (a) Using the triphenyl phosphite activator: Integral by line 1: Mn = 20660, Mw = 30434, PDI=1.41; Integral by line 2: Mn = 5151, Mw = 24998, PDI = 4.85. (b) Using the diphenyl isodecyl phosphite activator: Integral by line 1: Mn = 47219, Mw = 72709, PDI=1.54; Integral by line 2: Mn = 11095, Mw = 59322, PDI = 5.35.

5. NMR and Mass Data of Isolated products

5.1 NMR Data

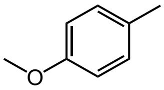

4-Methylanisole

^{1}H NMR (400 MHz, $CDCl_3$): δ (ppm) 7.08 (d, J = 8.2 Hz, 2H), 6.81 (d, J = 8.2 Hz, 2H), 3.77 (s, 3H), 2.28 (s, 3H). **^{13}C NMR** (100.6 MHz, $CDCl_3$): δ (ppm) 157.5, 129.9, 129.9, 113.7, 55.3, 20.5.

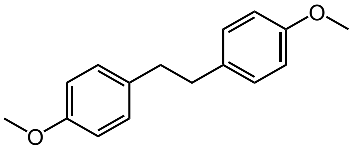

1,2-Bis(4-methoxyphenyl)ethane

^{1}H NMR (400 MHz, $CDCl_3$): δ (ppm) 7.07 (d, J = 8.6 Hz, 4H), 6.82 (d, J = 8.6 Hz, 4H), 3.78 (s, 6H), 2.82 (s, 4H). **^{13}C NMR** (100.6 MHz, $CDCl_3$): δ (ppm) 157.7, 133.9, 129.3, 113.6, 55.2, 37.2.

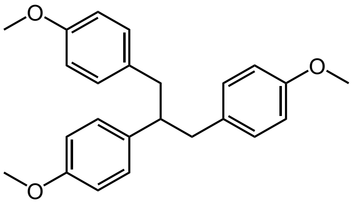

4,4',4''-(Propane-1,2,3-triyl)tris(methoxybenzene)

^{1}H NMR (400 MHz, $CDCl_3$): δ (ppm) 6.83 (dd, J = 16.4, 8.6 Hz, 6H), 6.65 (t, J = 8.1 Hz, 6H), 3.67 (s, 3H), 3.65 (s, 6H), 2.97 – 2.61 (m, 5H). **^{13}C NMR** (100.6 MHz, $CDCl_3$): δ (ppm) 157.8, 157.7, 136.5, 132.7, 130.1, 128.8, 113.5, 55.2, 55.2, 49.4, 41.7.

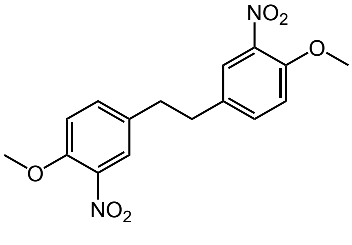

1,2-Bis(4-methoxy-3-nitrophenyl)ethane

^{1}H NMR (400 MHz, HFIP-d2): δ (ppm) 7.68 (d, J = 2.2 Hz, 2H), 7.36 (dd, J = 8.7, 2.3 Hz, 2H), 7.06 (d, J = 8.8 Hz, 2H), 3.90 (s, 6H), 2.89 (s, 4H). **^{13}C NMR** (100.6 MHz, HFIP-d2): δ (ppm) 152.1, 137.5, 136.3, 134.1, 125.6, 114.0, 55.8, 35.1.

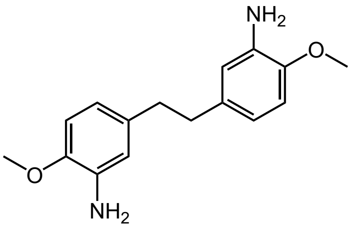

5,5'-(Ethane-1,2-diyl)bis(2-methoxyaniline)

^{1}**H NMR** (400 MHz, HFIP-d2): δ (ppm) 6.90 – 6.25 (m, 6H), 3.66 (s, 6H), 2.59 (s, 4H). ^{13}**C NMR** (100.6 MHz, HFIP-d2): δ (ppm) 147.1, 135.4, 130.9, 122.7, 118.2, 111.0, 54.7, 36.3.

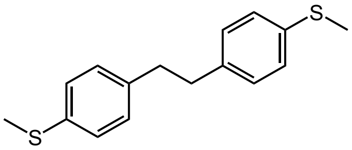

1,2-Bis(4-(methylthio)phenyl)ethane

^{1}**H NMR** (400 MHz, $CDCl_3$): δ (ppm) 7.18 (d, J = 8.3 Hz, 4H), 7.08 (d, J = 8.3 Hz, 4H), 2.85 (s, 4H), 2.46 (s, 6H). ^{13}**C NMR** (100.6 MHz, $CDCl_3$): δ (ppm) 138.7, 135.5, 129.0, 127.1, 37.3, 16.3.

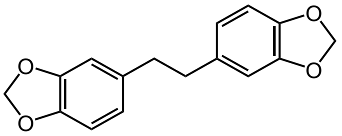

1,2-Bis(benzo[d][1,3]dioxol-5-yl)ethane

^{1}**H NMR** (400 MHz, $CDCl_3$): δ (ppm) 6.67 – 6.56 (m, 4H), 6.52 (dd, J = 7.9, 1.7 Hz, 2H), 5.84 (s, 4H), 2.71 (s, 4H). ^{13}**C NMR** (100.6 MHz, $CDCl_3$): δ (ppm) 147.5, 145.6, 135.4, 121.2, 108.9, 108.1, 100.8, 37.9.

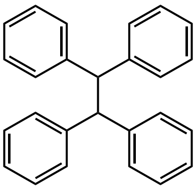

1,1,2,2-Tetraphenylethane

^{1}**H NMR** (400 MHz, $CDCl_3$): δ (ppm) 7.16 (d, J = 7.3 Hz, 8H), 7.09 (t, J = 7.6 Hz, 8H), 7.00 (t, J = 7.2 Hz, 4H), 4.77 (s, 2H). ^{13}**C NMR** (100.6 MHz, $CDCl_3$): δ (ppm) 143.4, 128.5, 128.1, 125.8, 56.3.

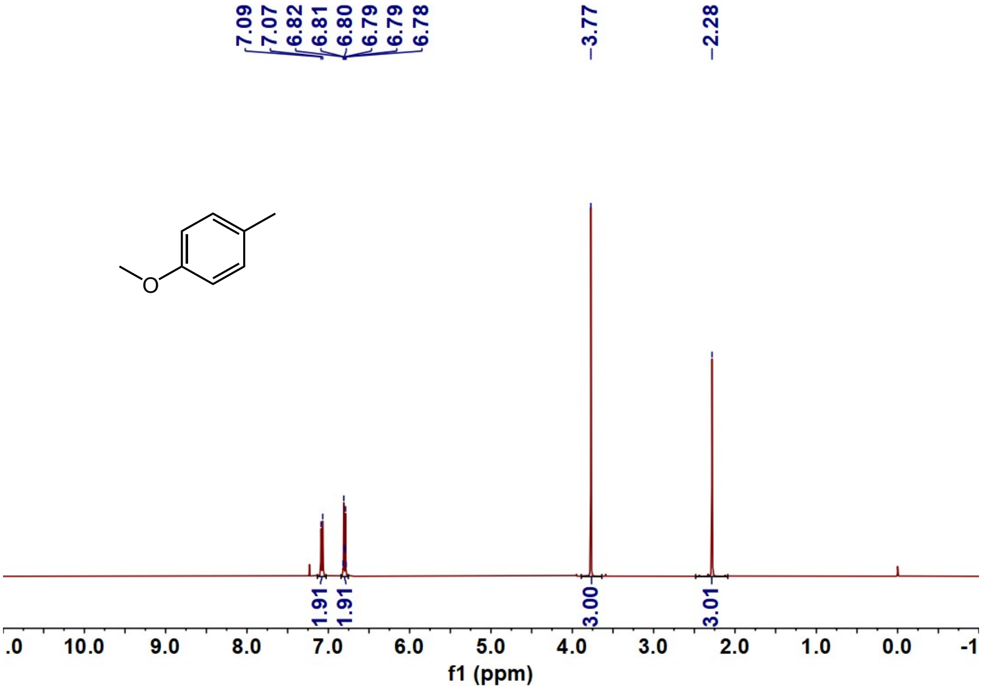
7.09
7.07
6.82
6.81
6.80
6.79
6.79
6.78
3.77
2.28
O
1.91
1.91
3.00
3.01
.0
10.0
9.0
8.0
7.0
6.0
5.0
4.0
3.0
2.0
1.0
0.0
-1
f1 (ppm)

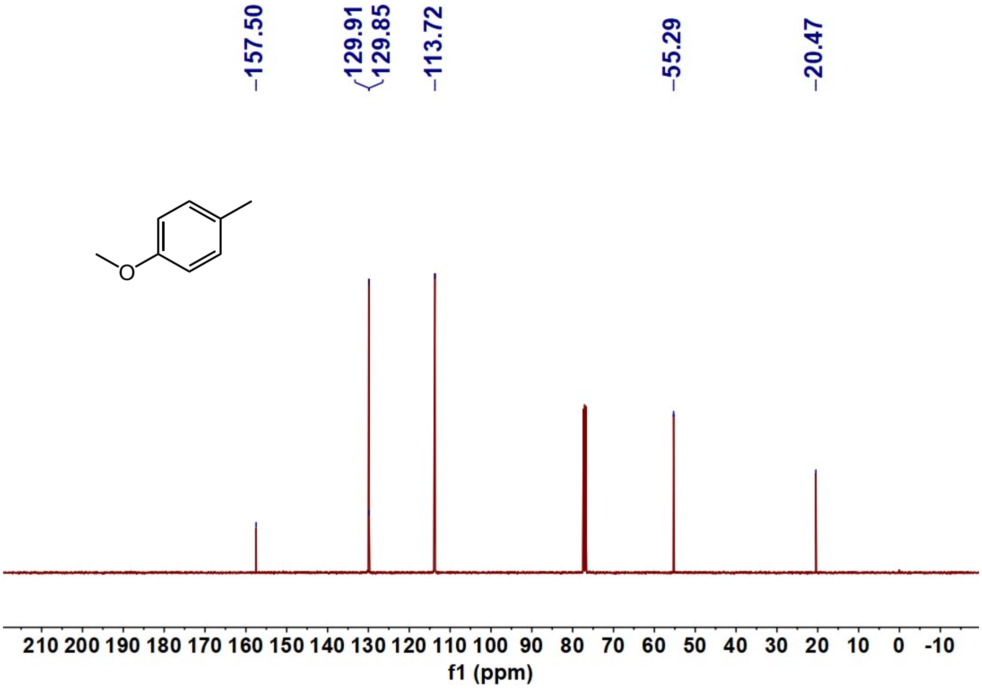
157.50
129.91
129.85
113.72
55.29
20.47
O
210
200
190
180
170
160
150
140
130
120
110
100
90
80
70
60
50
40
30
20
10
0
-10
f1 (ppm)

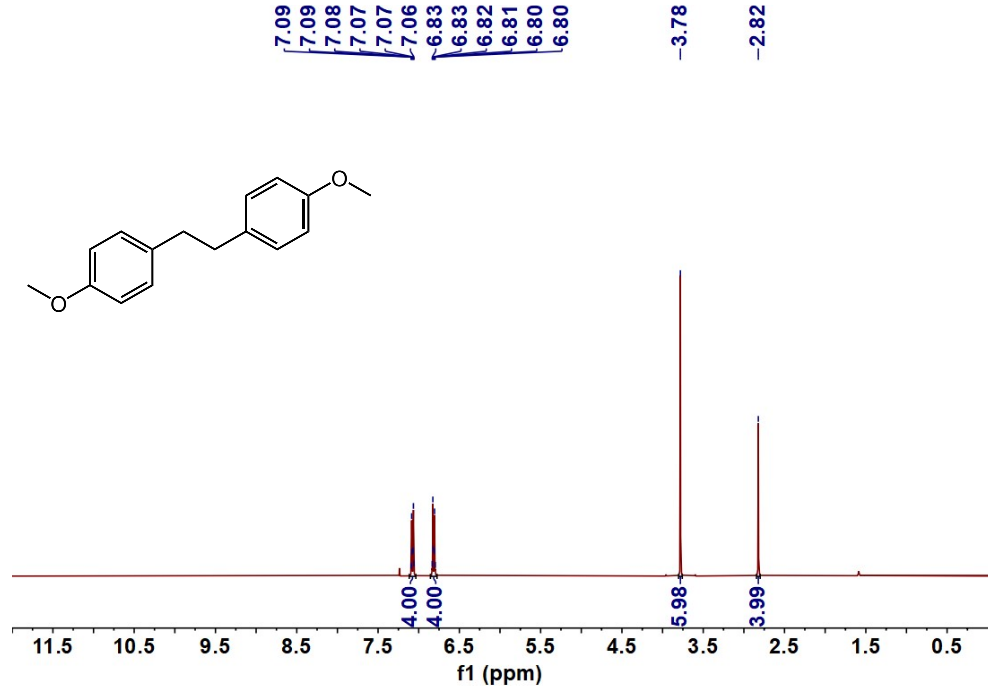
7.09
7.09
7.08
7.07
7.07
7.06
6.83
6.83
6.82
6.81
6.80
6.80
3.78
2.82
O
O
4.00
4.00
5.98
3.99
11.5
10.5
9.5
8.5
7.5
6.5
5.5
4.5
3.5
2.5
1.5
0.5
f1 (ppm)

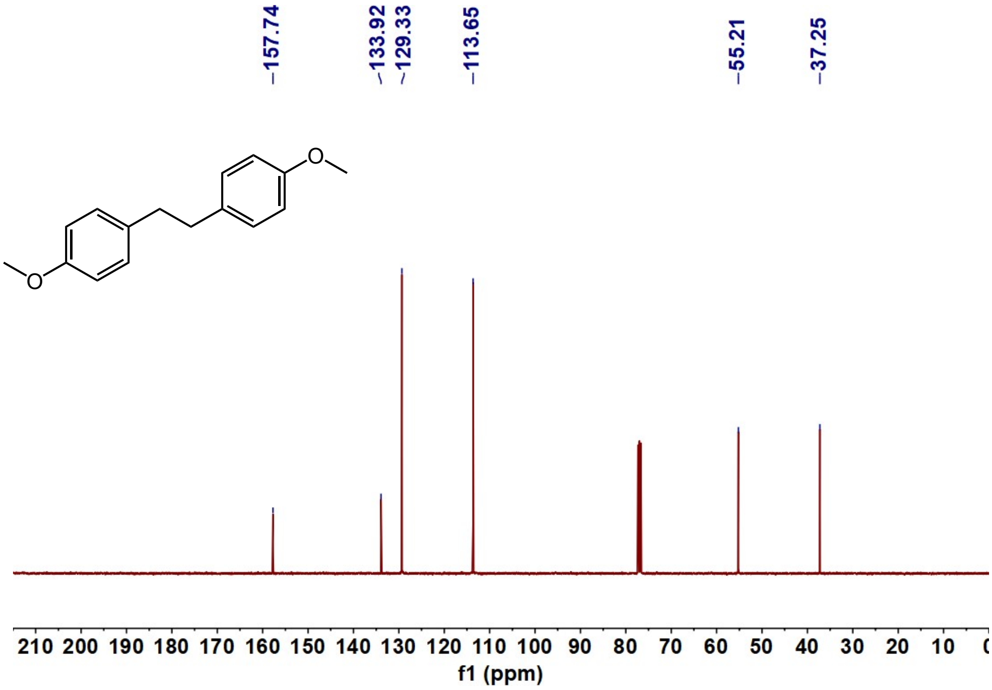
157.74
133.92
129.33
113.65
55.21
37.25
O
O
210
200
190
180
170
160
150
140
130
120
110
100
90
80
70
60
50
40
30
20
10
f1 (ppm)

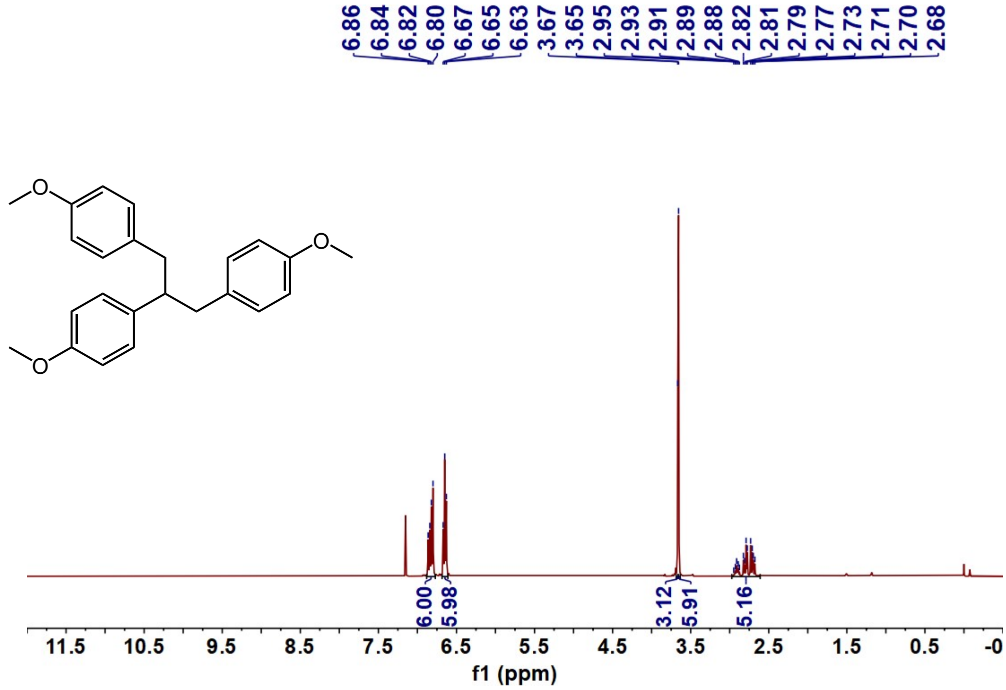
6.86
6.84
6.82
6.80
6.67
6.65
6.63
3.67
3.65
2.95
2.93
2.91
2.89
2.88
2.82
2.81
2.79
2.77
2.73
2.71
2.70
2.68
O
O
O
6.00
5.98
3.12
5.91
5.16
11.5
10.5
9.5
8.5
7.5
6.5
5.5
4.5
3.5
2.5
1.5
0.5
-0
f1 (ppm)

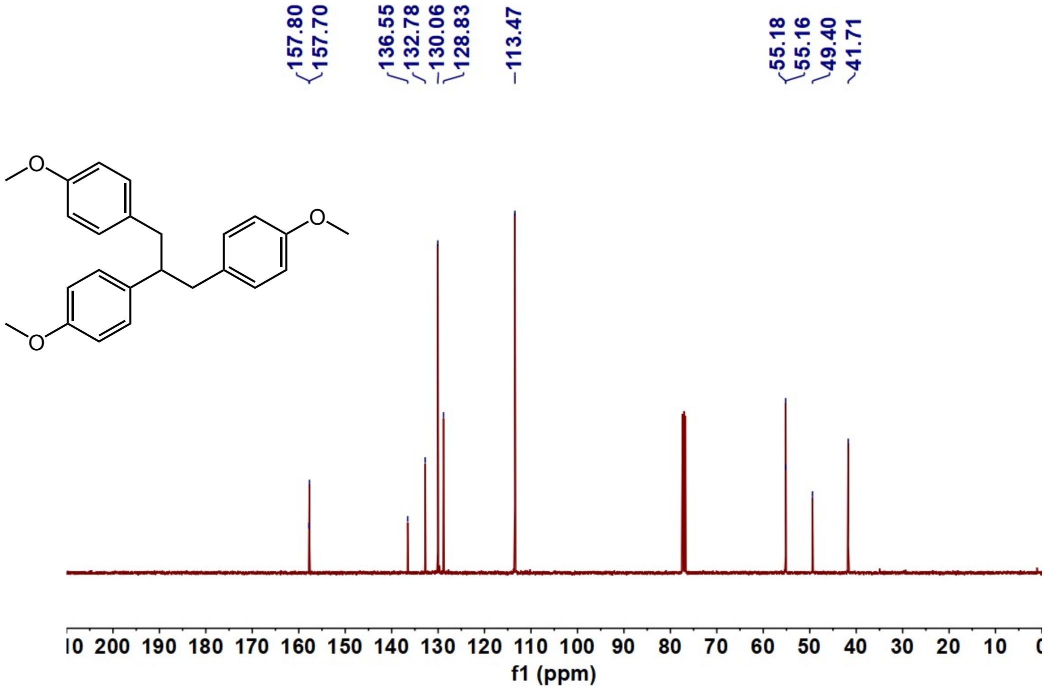
157.80
157.70
136.55
132.78
130.06
128.83
113.47
55.18
55.16
49.40
41.71
O
O
O
0
200
190
180
170
160
150
140
130
120
110
100
90
80
70
60
50
40
30
20
10
f1 (ppm)

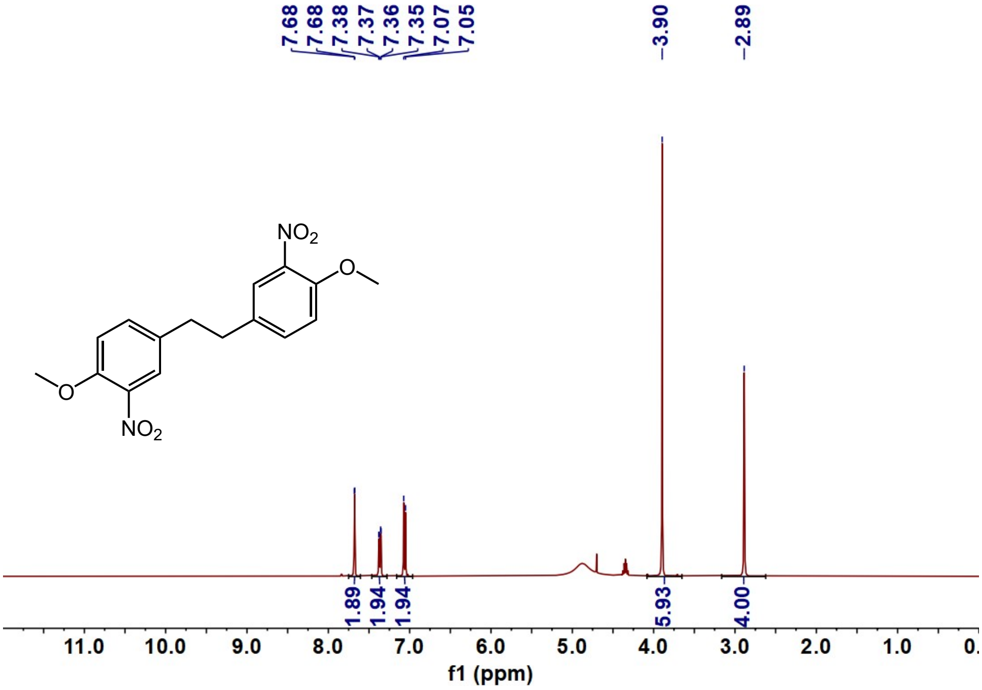
7.68
7.68
7.38
7.37
7.36
7.35
7.07
7.05
3.90
2.89
NO2
O
O
NO2
1.89
1.94
1.94
5.93
4.00
11.0
10.0
9.0
8.0
7.0
6.0
5.0
4.0
3.0
2.0
1.0
0.
f1 (ppm)

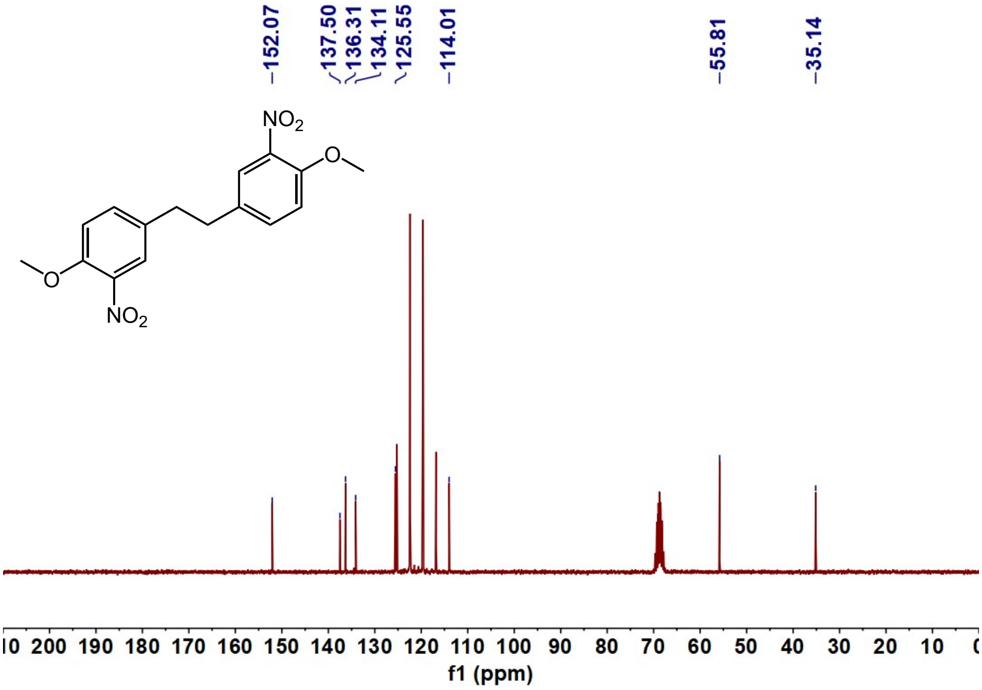
152.07
137.50
136.31
134.11
125.55
114.01
55.81
35.14
NO2
O
O
NO2
10
200
190
180
170
160
150
140
130
120
110
100
90
80
70
60
50
40
30
20
10
f1 (ppm)

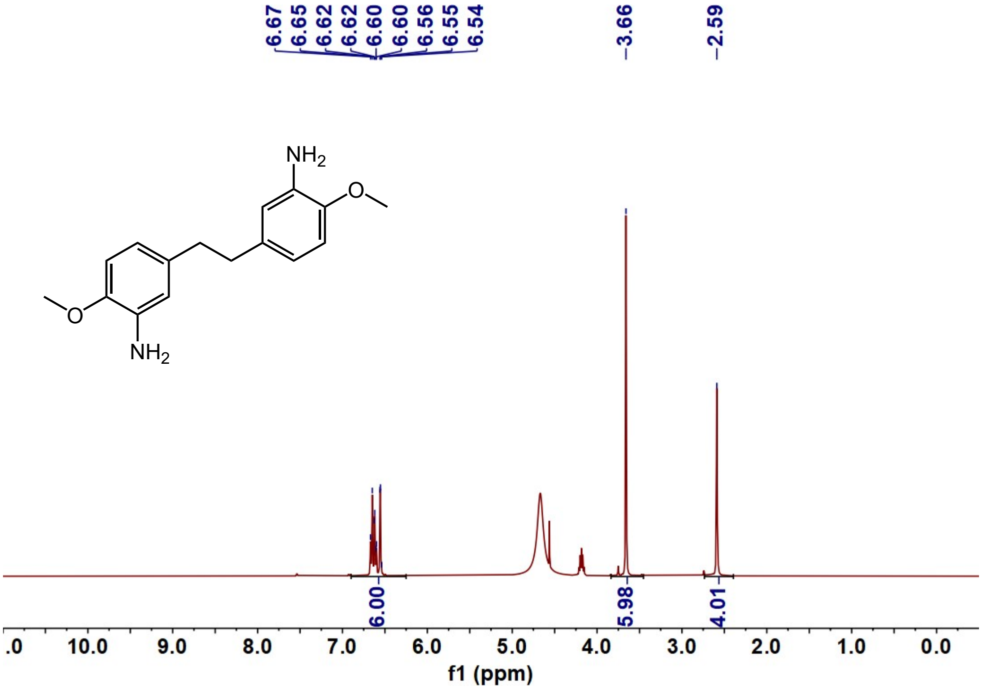
6.67
6.65
6.62
6.62
6.60
6.60
6.56
6.55
6.54
3.66
2.59
NH2
O
O
NH2
6.00
5.98
4.01
.0
10.0
9.0
8.0
7.0
6.0
5.0
4.0
3.0
2.0
1.0
0.0
f1 (ppm)

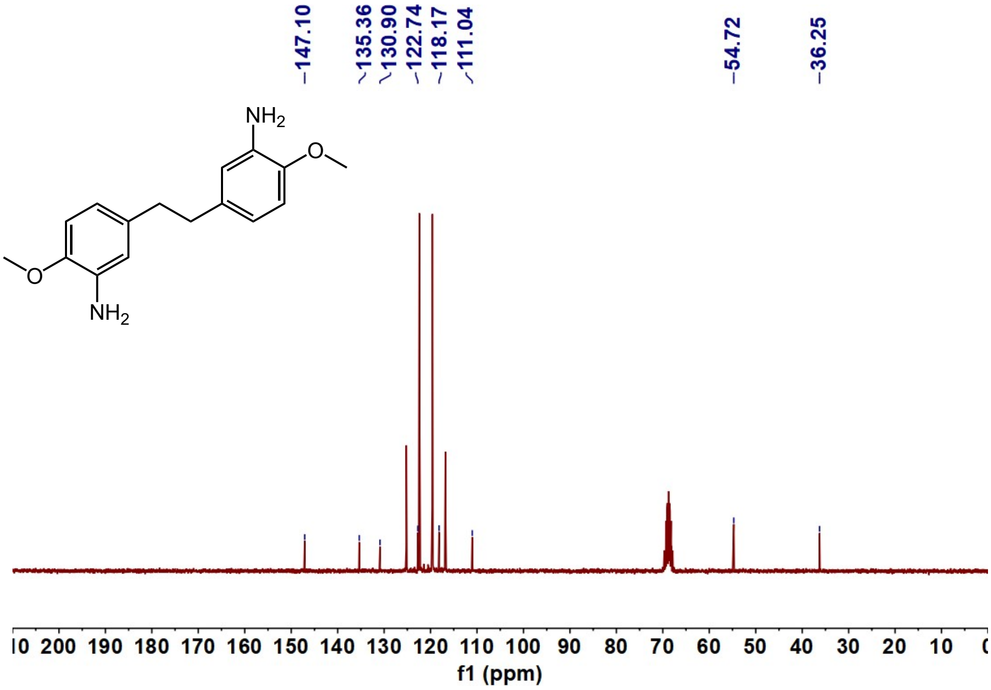
147.10
135.36
130.90
122.74
118.17
111.04
54.72
36.25
NH2
O
O
NH2
10
200
190
180
170
160
150
140
130
120
110
100
90
80
70
60
50
40
30
20
10
f1 (ppm)

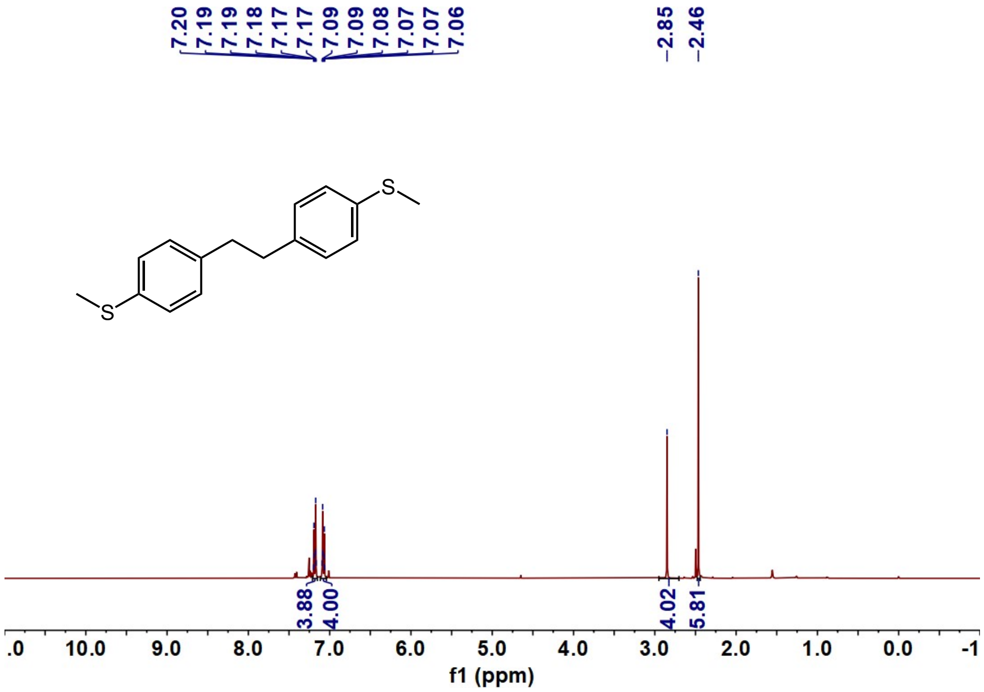
7.20
7.19
7.19
7.18
7.17
7.17
7.09
7.09
7.08
7.07
7.07
7.06
2.85
2.46
S
S
3.88
4.00
4.02
5.81
.0
10.0
9.0
8.0
7.0
6.0
5.0
4.0
3.0
2.0
1.0
0.0
-1
f1 (ppm)

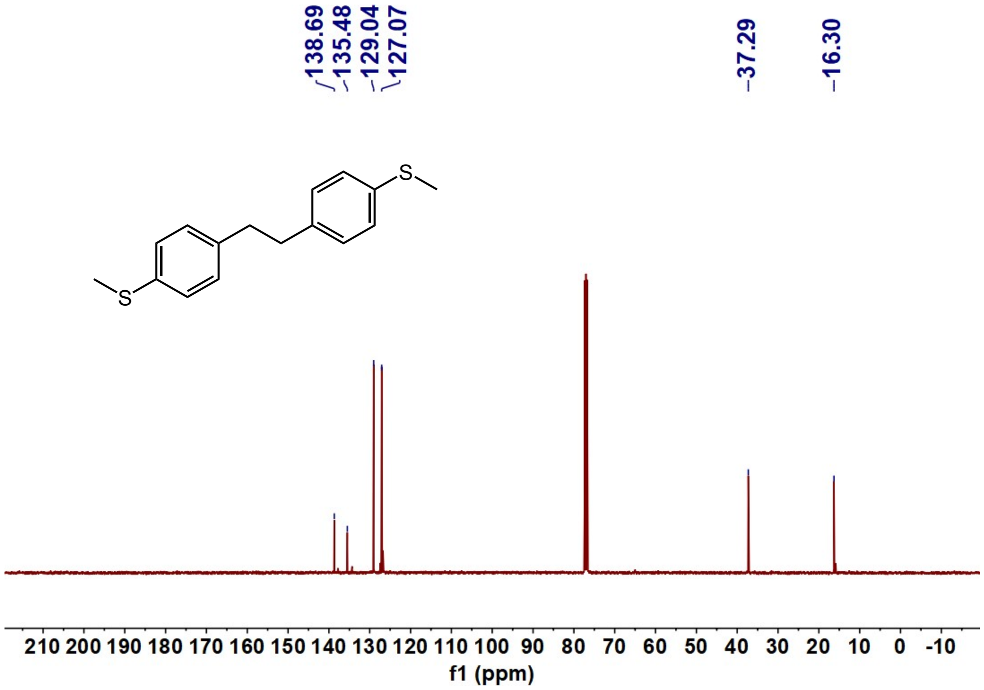
138.69
135.48
129.04
127.07
37.29
16.30
S
S
210
200
190
180
170
160
150
140
130
120
110
100
90
80
70
60
50
40
30
20
10
0
-10
f1 (ppm)

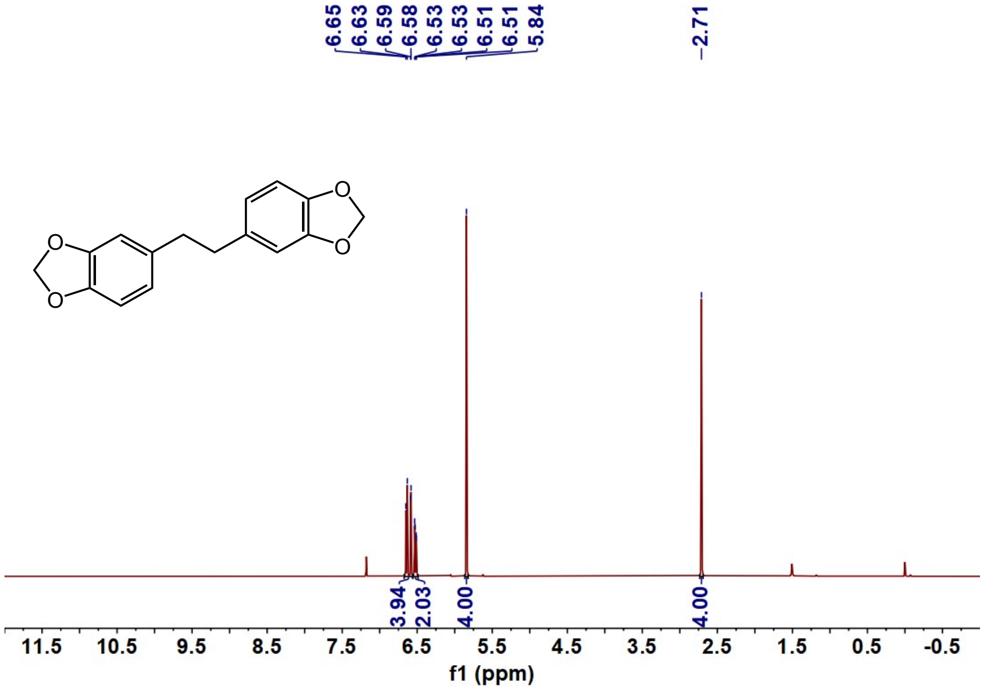
6.65
6.63
6.59
6.58
6.53
6.53
6.51
6.51
5.84
2.71
O
O
O
O
3.94
2.03
4.00
4.00
11.5
10.5
9.5
8.5
7.5
6.5
5.5
4.5
3.5
2.5
1.5
0.5
-0.5
f1 (ppm)

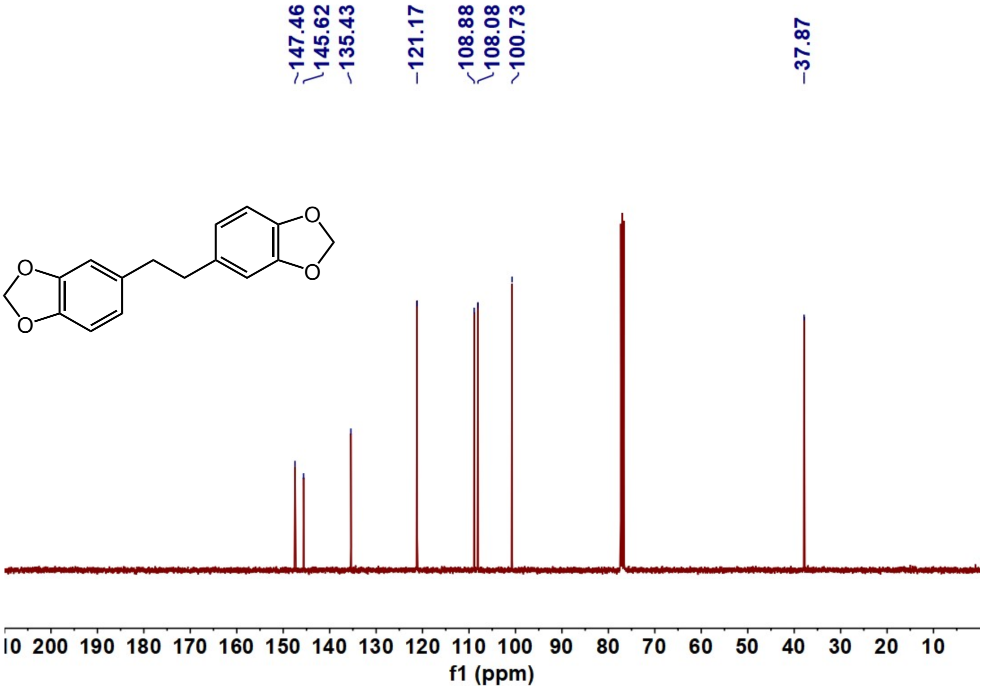
147.46
145.62
135.43
121.17
108.88
108.08
100.73
37.87
O
O
O
O
200
190
180
170
160
150
140
130
120
110
100
90
80
70
60
50
40
30
20
10
f1 (ppm)

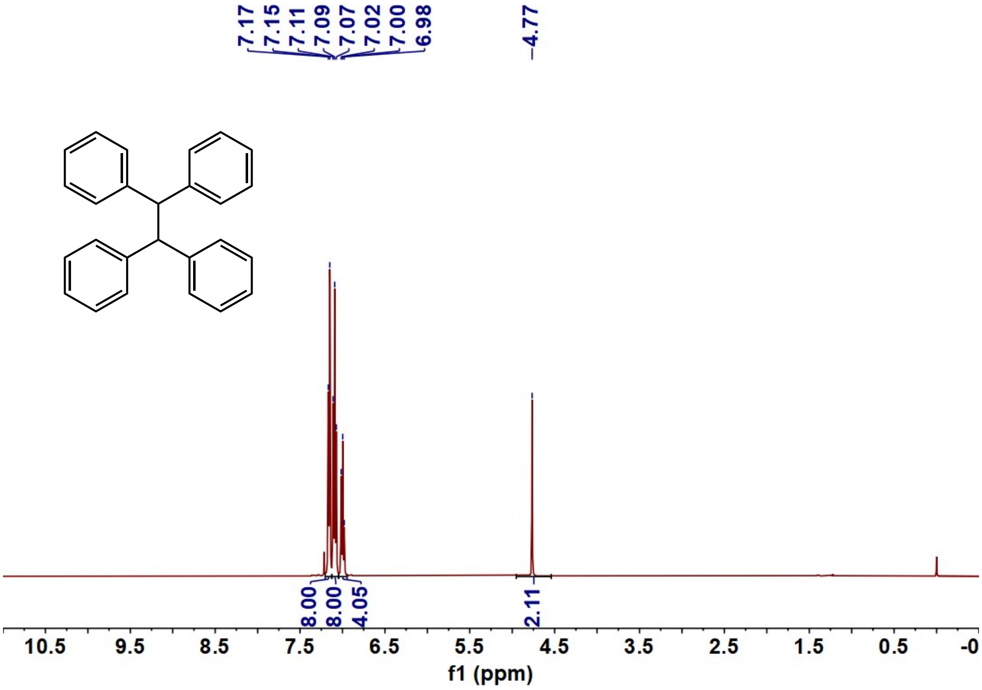
7.17
7.15
7.11
7.09
7.07
7.02
7.00
6.98
4.77
8.00
8.00
4.05
2.11
10.5
9.5
8.5
7.5
6.5
5.5
4.5
3.5
2.5
1.5
0.5
-0
f1 (ppm)

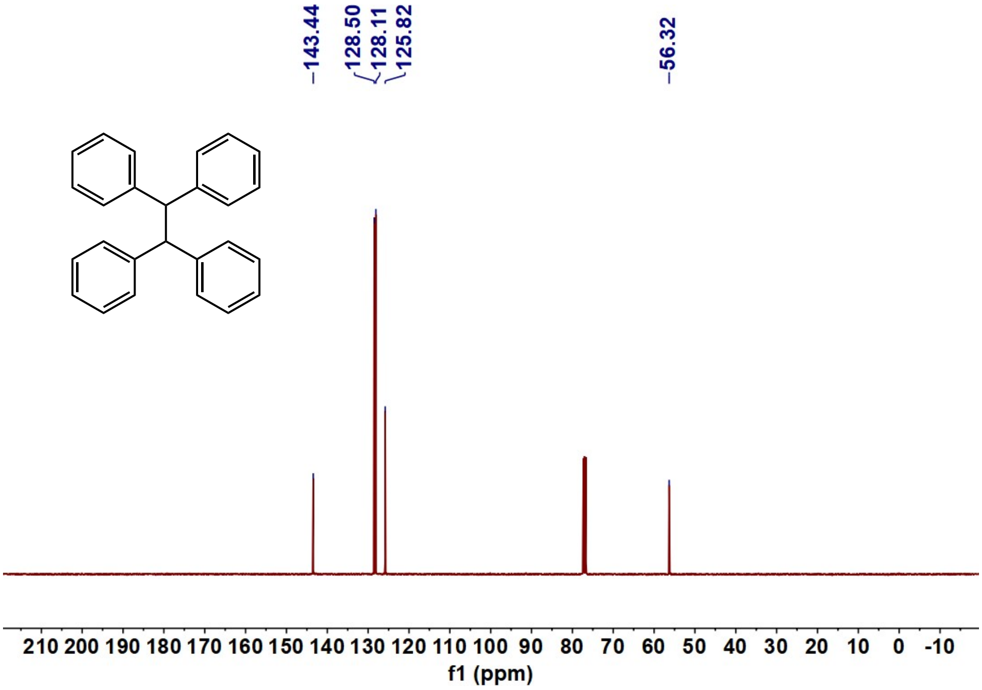
143.44
128.50
128.11
125.82
56.32
210
200
190
180
170
160
150
140
130
120
110
100
90
80
70
60
50
40
30
20
10
0
-10
f1 (ppm)

5.2 Mass Data (Horizontal axis: m/z; Vertical axis: relative abundance)

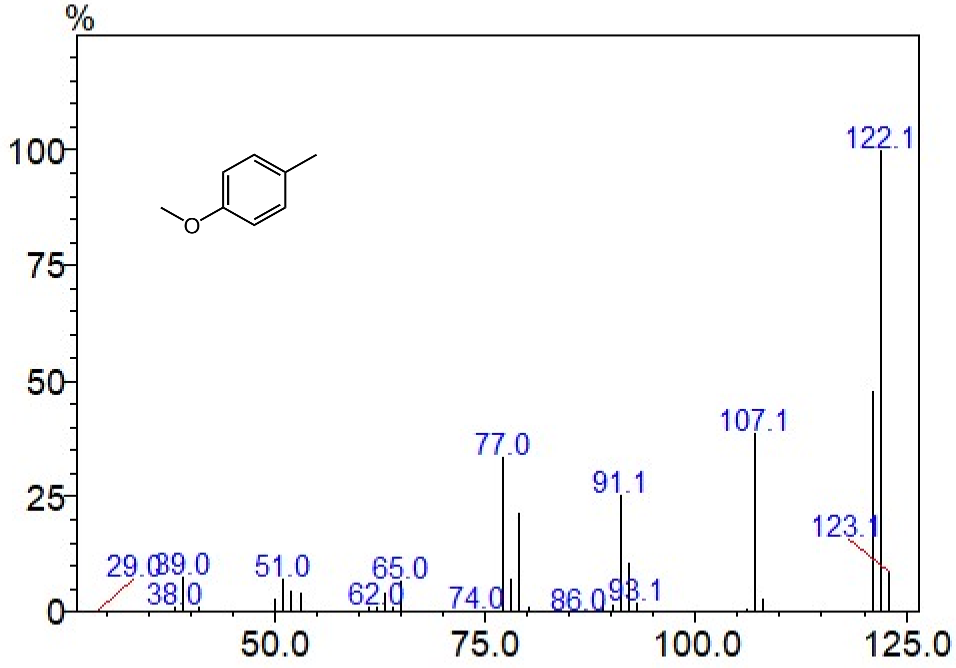

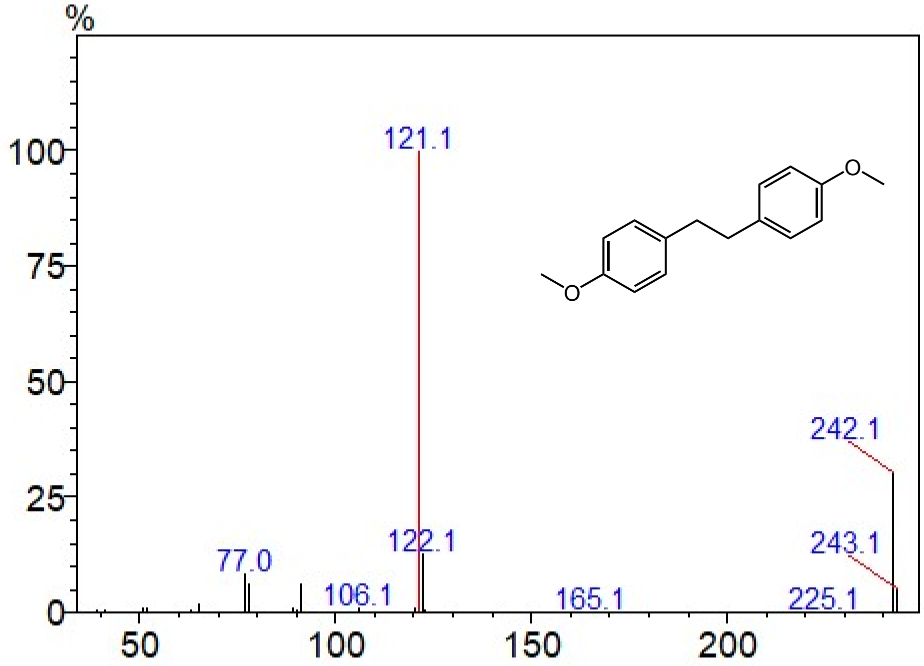

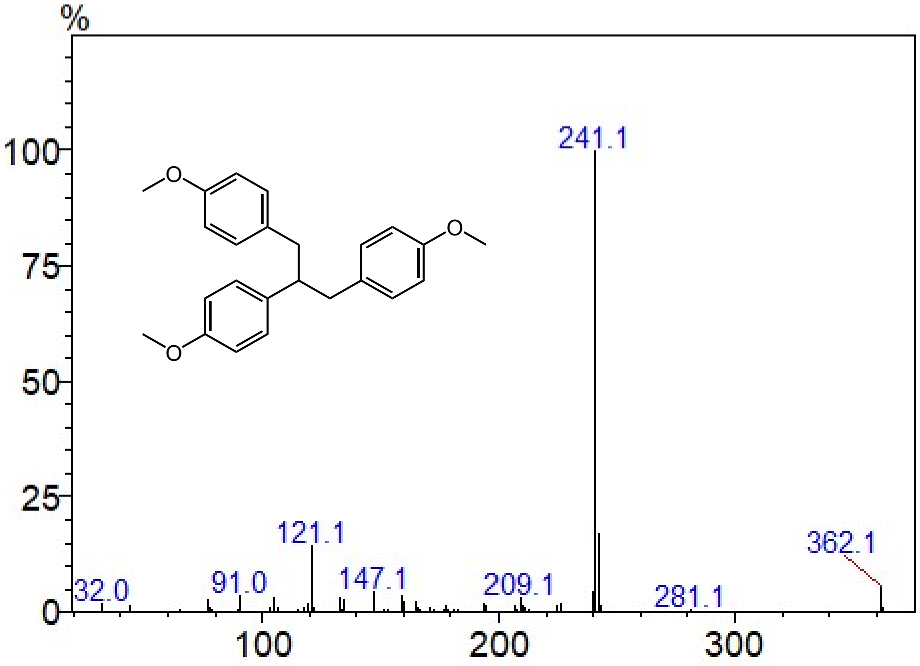
%
100
75
50
25
0
100
200
300
241.1
121.1
362.1
32.0
91.0
147.1
209.1
281.1
O
O
O

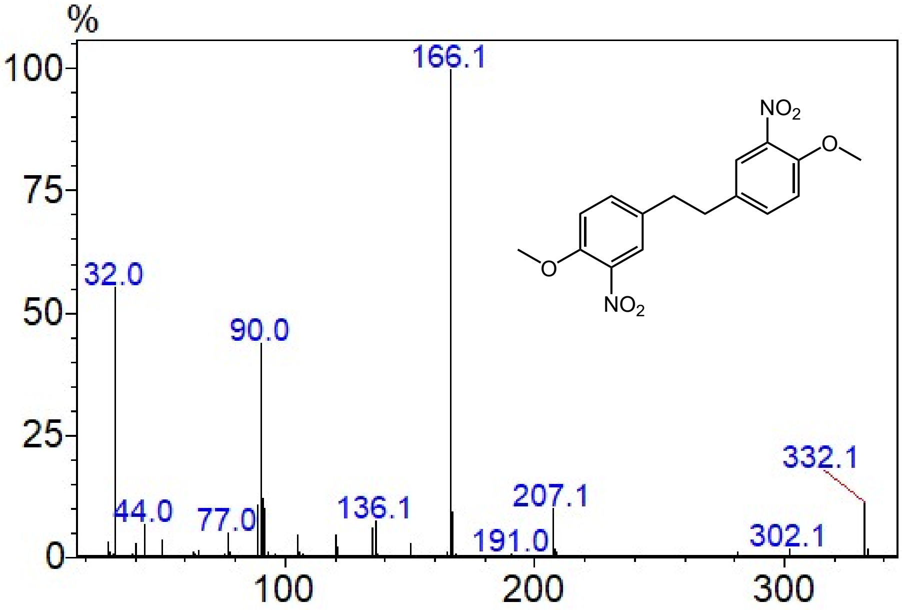
%
100
75
50
25
0
100
200
300
166.1
32.0
90.0
332.1
207.1
44.0
77.0
136.1
191.0
302.1
NO_2
O
O
NO_2

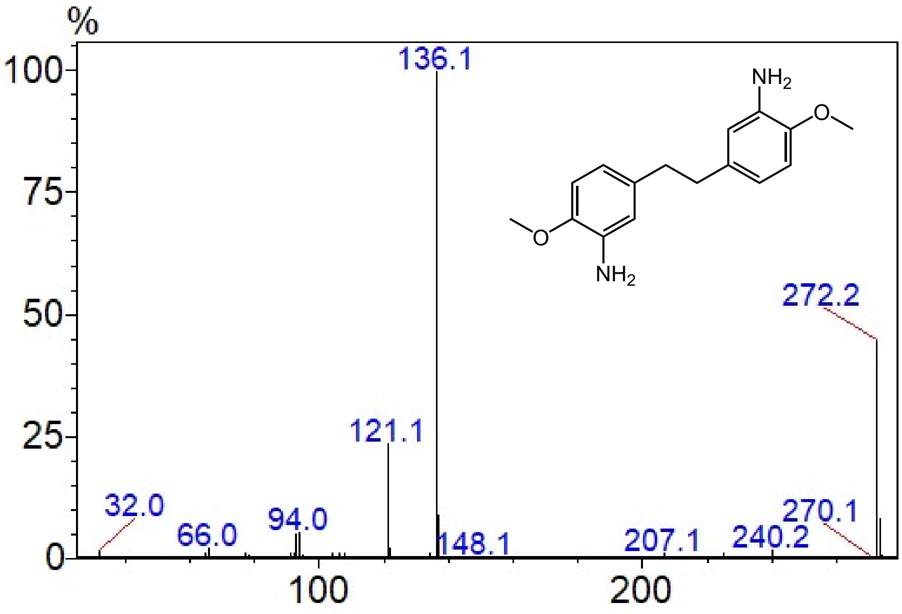
%
100
75
50
25
0
100
200
136.1
121.1
272.2
32.0
66.0
94.0
148.1
207.1
240.2
270.1
NH2
O
O
NH2

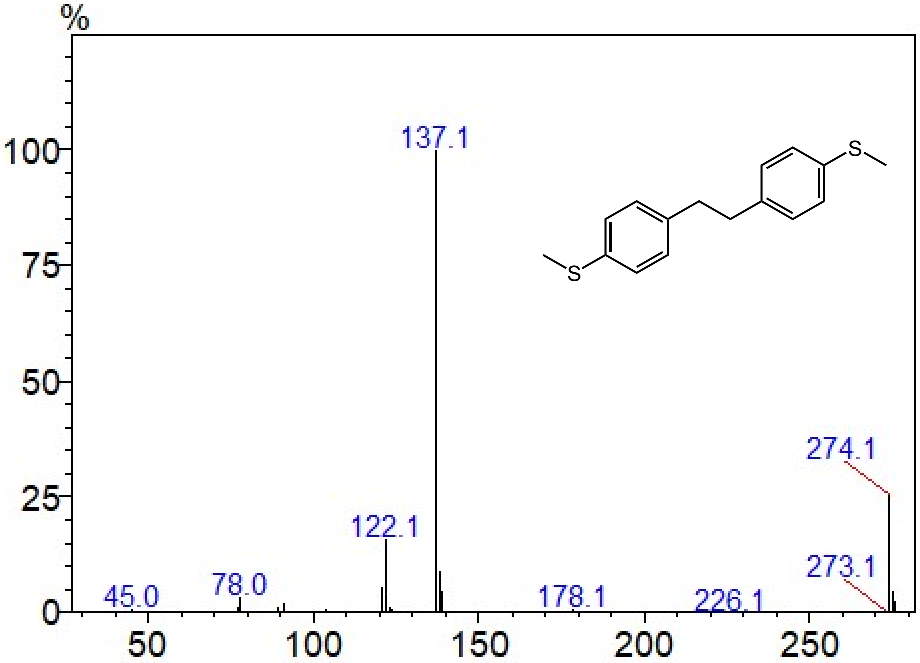
%
100
75
50
25
0
50
100
150
200
250
137.1
274.1
122.1
273.1
45.0
78.0
178.1
226.1
S
S

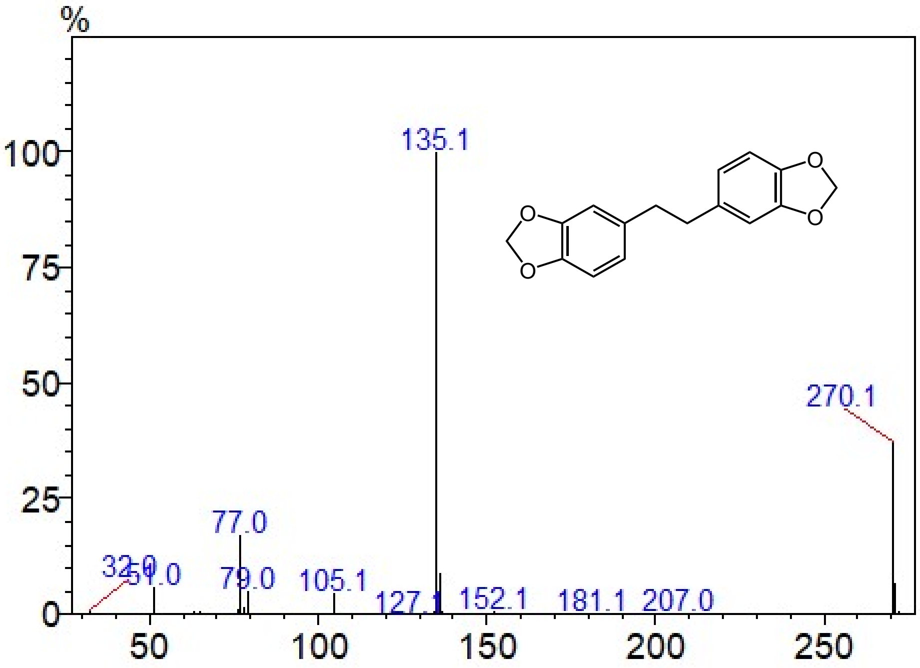

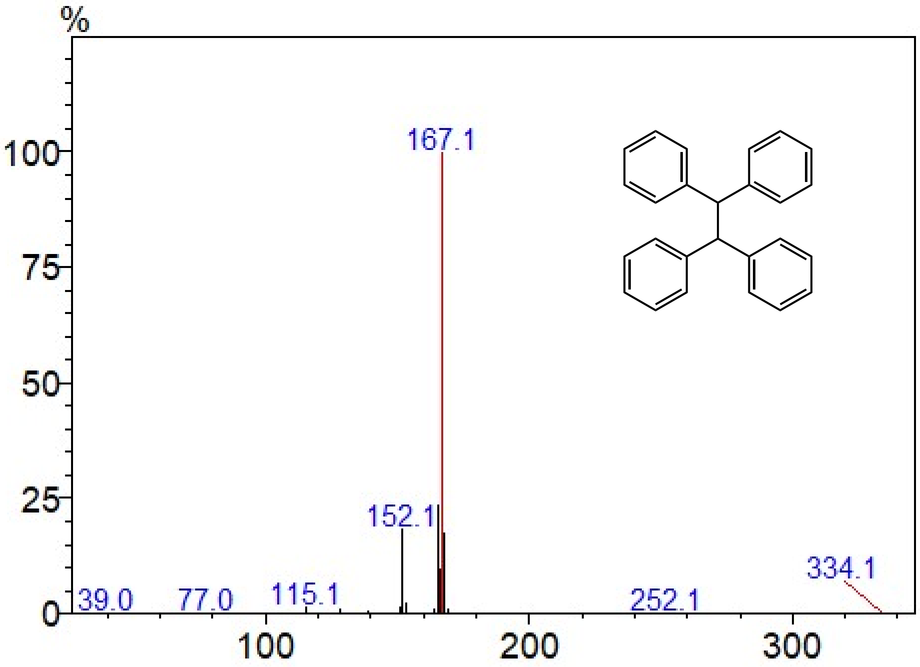

6. References

1 M. Lai, Z.-P. Bao, X. Qi and X.-F. Wu, *Org. Chem. Front.*, 2020, **7**, 3406–3410.

2 X. Ye, C. Yang, X. Pan, J. Ma, Y. Zhang, Y. Ren, X. Liu, L. Li and Y. Huang, *J. Am. Chem. Soc.*, 2020, **142**, 19001–19005.

3 Q. Wu, C. Shen, N. Rui, K. Sun and C. Liu, *J. CO_2 Util.*, 2021, **53**, 101720.

4 S. Coulton and I. François, *J. Chem. Soc., Perkin Trans. 1*, 1991, 2699–2705.

5 H. Zhou, Z. Chen, E. Kountoupi, A. Tsoukalou, P. M. Abdala, P. Florian, A. Fedorov and C. R. Müller, *Nat. Commun.*, 2021, **12**, 5510.

6 M. L. Poutsma, *Fuel*, 1980, **59**, 335–338.

7 B. A. Averill and W. H. Orme-Johnson, *Inorg. Chem.*, 1980, **19**, 1702–1705.

8 W. Zhan, X. Zhai, Y. Li, M. Wang, H. Wang, L. Wu, X. Tang, H. Zhang, B. Ye, K. Tang, G. Wang and M. Zhou, *ACS Nano*, 2024, **18**, 10312–10323.

9 H. Li, C. Tsai, A. L. Koh, L. Cai, A. W. Contryman, A. H. Fragapane, J. Zhao, H. S. Han, H. C. Manoharan, F. Abild-Pedersen, J. K. Nørskov and X. Zheng, *Nat. Mater.*, 2016, **15**, 48–53.

10 C. Lang, W. Jiang, C. Yang, H. Zhong, P. Chen, Q. Wu, X. Yan, C. Dong, Y. Lin, L. Ouyang, Y. Jia and X. Yao, *Small*, 2023, **19**, 2300807.

11 Q. Yuan, Y. Gu, W. Chen, Y. Zhang, X. Song, Y. Ding, X. Li, L. Zhu, Z. Jiang, L. Yan, J. Ma and Y. Ding, *Angew. Chem. Int. Ed.*, 2024, e202411632.